PFC/JA 86-49

Radial Profiles of Ground State Transitions of Helium-like Argon from the Alcator C Tokamak

J. E. Rice and E. S. Marmar

Plasma Fusion Center
Massachusetts Institute of Technology
Cambridge, MA 02139

E. Källne and J. Källne
JET
Abingdon, Oxfordshire, U.K.

August, 1986

Submitted to: Physical Review A

This work was supported by the U.S. Department of Energy Contract No. DE-AC02-78ET51013. Reproduction, translation, publication, use and disposal, in whole or in part by or for the United States government is permitted.

Radial Profiles of Ground State Transitions of Helium-like Argon from the Alcator C Tokamak

J. E. Rice and E. S. Marmar

Massachusetts Institute of Technology
Plasma Fusion Center
Cambridge, MA, U.S.A.

E. Källne and J. Källne
JET
Abingdon, Oxfordshire, U.K.

ABSTRACT

Spectra of the complete series of ground state transitions in helium like Ar^{16+} ($1snp-1s^2$, for $2 \leq n < 50$) have been obtained from the Alcator C tokamak using a compact x-ray crystal spectrometer. Radial profiles of these transitions have been measured and have been compared with the results of a transport model which includes the basic atomic processes. In the plasma center, collisional excitation is the most important population mechanism for the upper levels. For the outer regions of the plasma ($r/a_L > 0.5$), recombination of Ar^{17+} is the dominant population process for upper levels of most transitions, and preferentially populates the n = 2 triplet levels. Impurity transport provides sufficient amounts of hydrogen-like argon at the cooler, outer radii. For the high n transitions $1s9p-1s^2$ and $1s10p-1s^2$, charge exchange recombination is the dominant population mechanism at the plasma edge under certain operating conditions. The intensities of these lines have been used to determine neutral hydrogen density profiles. For ground state transitions with n > 13, charge transfer from excited neutral hydrogen is the only important population process for $r/a_L > 0.5$.

I. Introduction

Recently, there has been considerable interest in x-ray spectroscopy of highly ionized atoms in high temperature tokamak plasmas.[1-17] Of particular interest are $\Delta n = 1$ x-ray spectra from helium-like species of medium Z impurities.[4,5,7,8,10-15] Most measurements on tokamaks have been obtained using large spectrometers with Rowland circle geometry, which because of size constraints, are restricted to view along central chords. In the center of high temperature plasmas, electron impact excitation is the most important mechanism for populating the upper levels of the observed transitions. For the measurements described in this paper, x-ray spectra of helium-like Ar^{16+} have been obtained with a compact spectrometer of Von Hamos geometry, which has been scanned radially to obtain spectra from all regions of the plasma, including the edge. In the regions of the plasma where the electron temperature is much lower than the transition energy, radiative recombination of Ar^{17+} is the most important process for populating most of the upper levels in Ar^{16+}. The key to the existence of this condition is that the outward radial transport time of Ar^{17+} from the hot plasma core is comparable to the recombination times, so that hydrogen-like argon exists in the very cool regions near the edge. Also near the plasma edge, where the neutral hydrogen density is relatively high, charge transfer recombination is found to be very important in populating certain levels in Ar^{16+} both by direct recombination and through subsequent cascades.

The spectrometer system and experimental conditions are described in Section II. Ground state transitions of helium-like argon from the n = 2 level, in addition to several satellite lines, have been identified and are presented in Section III. Radial brightness profiles of the Ar^{16+} emission features have been measured and are shown in Section IV. Section V is devoted to the modelling of the radial brightness profiles of the four main lines in the helium-like spectrum. Radial profiles of ground state transitions from high n levels ($3 < n < 13$) in helium-like argon and observations of charge exchange recombination are shown in Section VI. Determination of the neutral hydrogen density profile is described in Section VII. In Section VIII are presented observations of very high n ($15 < n < \infty$) transitions to the ground state in Ar^{16+}. Radial profiles of satellite transitions are shown in Section IX.

II. Spectrometer system and Experimental Conditions

X-ray spectra from highly ionized argon Refs. [7,8,12,14-17] have been obtained from the Alcator C Ref. 18 tokamak using a compact x-ray crystal spectrometer. The spectrometer system has been described in detail elsewhere [14,19] and some relevant features are summarized here. The Von Hamos type instrument was employed with a 2.5 cm × 2.5 cm quartz crystal (2d = 6.687 Å) and a radius of curvature of 50 cm. The X-rays were dispersed onto a five wire, linear position sensitive delay line proportional counter wtih an active area of 3.5 cm × 1.0 cm, which utilized a krypton-ethane gas flow. The wavelength range from 2900 mÅ to 4100 mÅ was available for the configuration used in these experiments, with a 100 mÅ bite for each spectrometer setting. Large composite spectra were then obtained by adding several overlapping spectra. Individual lineshapes were dominated by doppler broadening broadening as the resolving power of the spectrometer was 2500. Due to the compact size of the instrument, radial (vertical) scans could be performed by tilting in a plane perpendicular to the toroidal magnetic field. The spatial resolution of ± 1.5 cm was determined largely by the slit height. The spectrometer was able to be scanned in chord height, d, from the plasma centered ($d = 0$) to outside the limiter radius ($d > a_L$).

Measurements described in this paper were from plasmas with limiter radii, a_L, of 12.5 and 16.5 cm. The toroidal magnetic field was in the range from 80 to 100 kG, hydrogen, deuterium and helium working gases were used, and the average electron density was in the range from 1.0 to 2.5 $10^{14} cm^{-3}$. Density profiles were taken to have the form $n_e = n_{eo} (1-(r/a_L)^2)^\alpha$ with α in the range from 0.5 to 1.0. Electron temperature profiles were of the form $T_e = T_{eo} \exp -(r/a_T)^2$ where a_T generally depends on plasma parameters as $a_T^2 = 3/2\ q_o/q_L\ a_L^2$ with q_o and q_L the central and limiter safety factors.

Argon was introduced into the torus through a fast piezo-electric value. The argon subsequently recycled and reached a steady state level in the plasma for typically a 200 ms duration, during which time the measurements were made. Concentrations were in the range from 10^{-5} to 10^{-3} of the electron density.

III. Δ n = 1 Spectra of He-like Argon

In Fig. 1 is plotted a spectrum of Ar^{16+} taken from several similar discharges with $\bar{n}_e = 2.4 \times 10^{14}$ cm^{-3}, T_{eo} = 1650 eV, B_T = 80 kG and I = 275 kA. The strongest lines are the resonance (w, 3.948Å), forbidden (z, 3.993Å) and intercombination lines (x, 3.965Å and y, 3.968Å)[7,8], and several satellite transitions from lithium-like (with the spectator electron in the n = 2, 3 and 4 levels) and beryllium-like argon are also seen. In the lower portion of the figure is a logarithmic plot of the data in addition to the fitted spectrum. The line shapes are assumed to be Gaussian and the fitting routine determines the amplitude, width and position of a specified number of lines in the spectrum. The ion temperatures and hence the line widths are taken to be the same for all the lines. Measured and theoretical[12,20,21] wavelengths and configurations for several transitions are given in Table 1. No direct wavelength calibration has been made for these spectra so the quoted values are normalized to the theoretical values[20] for the resonance and forbidden lines.

IV. Radial Profiles of Δ n = 1 Transitions in He-like Argon

Radial brightness profiles have been obtained by vertically scanning the spectrometer on a shot to shot basis. Shown in Fig. 2a-2d are spectra taken at several radial locations for a series of identical 80 kG, deuterium discharges with a_L = 12.5 cm. The top spectrum was obtained from the central chord where the central electron temperature was 1650 eV, and is indicative of normal operating conditions. In the second spectrum, taken at a chord height of 8 cm, the forbidden line is stronger than the resonance line and the satellites have also grown relative to w. The electron temperature was down a factor of three at 8 cm. In the third spectrum, at a chord of 10.5 cm, the forbidden line dominates, and the satellites have disappeared. At 10.5 cm the temperature was about 250 eV. Nearly all that remains in the bottom spectrum is the forbidden line. This was obtained near the limiter radius where the electron temperature was about 100 eV. The spatial resolution of the instrument is ~ 3 cm. The lines are narrower at the outer radii due to a decrease in the ion temperature as evidenced by the increase in the valley between the intercombination lines for successive spectra.

Shown in Fig. 3 are radial brightness profiles for the major components of the helium-like argon spectrum from the series of identical discharges from which the spectra of Fig.2 were obtained. The profiles were determined from the integrated intensities of the fitted spectra. The resonance line has the narrowest radial profile, and crosses the forbidden line profile at 8.0 cm and the intercombination line profiles at 9.8 cm. The forbidden line has the broadest radial profile. The overlapping satellite j has been subtracted from z using a constant factor of 1.3 times the intensity of k[8]. The intercombination line profiles steadily converge with increasing radius. Plasma parameters for this series of discharges were Teo = 1650 eV, aT = 7.5 cm, aL = 12.5 cm, neo = 3.5×10^{14} cm^{-3} and α =1.0.

V. Population Mechanisms and Predicted Profiles

In an attempt to account for these observed brightness profiles, a model for helium-like line intensities has been used[22]. Modelling of the relative intensities of lines from central chord measurements has previously been reported[11-13]. Populations of the various levels are determined by a balance among radiative transitions, collisional excitation and de-excitation, radiative and dielectronic recombination and collisional innershell ionization and excitation. The n = 3 and above levels are treated as part of the continuum and interactions with an external radiation field are ignored. Transition probabilities and the appropriate ionization, recombination and excitation rate coefficients have been taken from Ref. 22 and 23. In order to determine the density of helium-like argon ions with one electron in an excited n = 2 level, the densities of helium-, hydrogen- and lithium-like argon in their respective ground states must first be known. As an example, in Fig. 4a are shown the fractional abundances (proportional to the radial density profiles) of various charge states of argon, (normalized to the flat total argon density) assuming that coronal equilibrium obtains. The same electron density and temperature profiles mentioned at the end of Section IV have been used in the calculations. The Ar^{16+} profile is relatively flat out to 8 cm and then rapidly falls off. The Ar^{17+} profile is centrally peaked while the Ar^{15+} profile is hollow with a maximum in the shell structure near 8.5 cm.

The radial brightness profiles may now be calculated. As a starting point, it is assumed that electron impact excitation from the ground state of Ar^{16+} is the only population mechanism for the n = 2 levels. Again, measured electron density and temperature profiles as mentioned above are used, and the instrumental spatial resolution of 3 cm has been folded in. The calculated brightness profiles for the resonance, intercombination and forbidden lines are shown in Fig. 5a for the charge state profiles of Fig. 4a. The profiles of the four lines are much narrower than the observed profiles of Fig. 3 and do not exhibit the crossing of the triplet profiles by the resonance line (singlet) profile. Inclusion of dielectronic and radiative recombination as upper level population processes does not substantially improve matters, as shown in Fig. 5b, mainly because of the lack of sufficient hydrogen-like argon at the outer radii (as shown in Fig. 4a), for the recombination to occur. There is however about a factor of two increase of the triplet lines relative to the resonance line.

From impurity transport studies performed on Alcator C[24], it is known that radial transport times can be shorter than certain recombination times. In fact, the diffusion coefficients used to describe the observed impurity transport are much greater than the theoretical neoclassical values. This would imply that impurity transport can cause charge state distributions to depart seriously from the coronal equilibrium values. This is demonstrated in Fig. 4b, where the ionization state density profiles calculated from an impurity transport code, using an anomalous impurity diffusion coefficient of 1500 cm^2/sec (consistent with the results of Ref. 24), are shown for comparison. The densities of helium-, lithium- and beryllium-like argon are similar for the two cases inside a radius of 8 cm, but at 10 cm, the helium-like density for the case with transport is four orders of magnitude higher than the coronal equilibrium case. The hydrogen-like density profiles are similar inside 3 cm for the two figures, but the transport case is 1000 times larger at 8 cm. At 10 cm the discrepancy is about 8 orders of magnitude. This indicates that impurity transport is an important consideration when interpreting brightness profiles, especially when recombination of Ar^{17+} is significant.

Shown in Fig. 6a are the predicted brightness profiles when anomalous impurity transport is included in the calculation of the charge state density profiles, and when the only population mechanism of the n = 2 levels is collisional excitation. Again, these profiles do not agree with the observations. Shown in Fig. 6b are the brightness profiles for the resonance, intercombination and forbidden lines when radiative and dielectronic recombination are included as population processes for excited n = 2 levels in Ar^{16+}. While there is little change of the profiles inside of 6 cm, the brightnesses are greatly enhanced in the cooler regions of the plasma. The forbidden and intercombination line brightness profiles are predicted to be broader than the resonance line profile, in agreement with the observations. The conclusion is that in the outer regions of the plasma, recombination is the dominant population mechanism for the n = 2 triplet states, and this is only possible because the impurity transport effects provide hydrogen-like argon in sufficient quantities.

While there is qualitative agreement between the model predictions and the observations, the relative intensities of the resonance and forbidden lines are not exact, as the crossing point is observed to occur near 8 cm instead of at 9 cm as predicted. If the recombination rate coefficients are all increased by a factor of 5, the relative intensities are in quantitative accord, as shown in Fig. 7b. In Fig. 7a, the observed profiles of Fig. 3 are reproduced on the same scale for comparison. It is possible that the recombination rates of Ref. are too small, although it is likely that the treatment of all levels with n = 3 and above as part of the continuum is a possible source of the disagreement since cascades to different n = 2 levels following recombination into higher n levels have not been properly treated[25]. There are also uncertainties in the hydrogen-like argon density profiles calculated from the impurity transport code which could affect the the size of the contribution from radiative recombination. These uncertainties arise from uncertainties in the possible spatial variation in the diffusion coefficient and in the electron temperature profile. It has been suggested[8] that charge-exchange recombination is a process that can be important for populating the n = 2 triplet levels following cascades from higher n levels. In the following section are presented direct observations of charge exchange recombination which may have a bearing on the profiles of Δ n = 1 transitions in Ar^{16+}.

VI. High n Spectra of Ar^{16+} and Charge Exchange Recombination

Shown in Fig. 8 is a spectrum of the 1snp - $1s^2$ series in Ar^{16+} in the wavelength region from 3.0 to 3.4 Å for n between 3 and 13. Plasma parameters for the hydrogen, 80 kG discharges for which this spectrum was obtained were I_p = 410 kA, $\bar{n}_e = 2.2 \times 10^{14}$ cm^{-3} and T_{eo} = 1500 eV. Wavelengths for the lines 1s5p- to 1s10p-$1s^2$ have been taken from Ref.. Several satellites are apparent between 3.1 and 3.3 Å, and are discussed in Section IX. Wavelengths, relative intensities and line identifications are given in Table 2[27-29]. The relative intensities of the 1snp - $1s^2$ series for the central chord measurements are shown in Fig. 9 and are in agreement with the relative magnitude of the oscillator strengths[30] ($\propto n^{-3}$) which indicates that electron impact excitation is the predominant mechanism for populating the upper levels. Shown in Fig. 10 are spectra from 1s7p - $1s^2$ to 1s11p - $1s^2$ transitions obtained at three different radial locations for a series of 80 kG, hydrogen discharges with a limiter radius of 16.5 cm. For the outer radii, the 1s9p - $1s^2$ and 1s10p - $1s^2$ lines are strongly enhanced relative to 1s7p - $1s^2$, compared to the central spectrum[16]. This suggests that there is a population mechanism which selects these particular levels. Charge transfer between neutral hydrogen and hydrogen-like argon should selectively populate levels around n = 9 and n = 10, since Ar^{17+} is similar to fully stripped chlorine[31]. This process will be important in the cooler regions of the plasma where there is a large relative neutral density. By measuring the enhancement of the 1s9p - $1s^2$ and 1s10p - $1s^2$ transitions over the values expected from population by excitation and radiative recombination, the intrinsic neutral density and density profile can be determined provided the charge transfer cross sections are known. Enhanced population of high n levels in oxygen by charge-exchange recombination with intrinsic n_o has been observed previously in ORMAK [32].

The situation is different in helium working gas. In contrast to the hydrogen case, spectra obtained in He^4 do not exhibit a strong enhancement of the 1s9p - and 1s10p - $1s^2$ transitions at the outer radii, as shown in Fig. 11. This is because there is no resonant transfer between neutral helium and Ar^{17+} into levels near n = 9.

Brightness profiles for the transitions 1s3p - $1s^2$ to 1s12p -$1s^2$, obtained during a series of 80 kG, hydrogen discharges with $\bar{n}_e = 1.8 \times 10^{14} cm^{-3}$ and T_{eo} = 1800 eV are shown in Fig. 12. The limiter radius was 16.5 cm. All of the profiles are centrally peaked and rapidly fall off in intensity out to a chord of 8 cm. Outside of 8 cm, all the profiles tend to flatten out. The 1s9p - and 1s10p - $1s^2$ profiles cross the 1s8p - $1s^2$ curve at about 8 cm, while all the other profiles have a similar shape. A model similar to the one described in Section IV has been used to calculate the emissivity (and brightness) profiles of the 1snp - $1s^2$ series for $3 < n < 13$. The line intensities are determined from a balance among radiative decay directly to the ground state, collisional excitation out of the ground state of helium-like argon, and radiative and charge exchange recombination of hydrogen-like argon in the ground state. In general, the emissivity of a 1snp - $1s^2$ transition in Ar^{16+} is given by

$$E_n (r) = n_e(r) \left[n_{Ar^{16+}}(r) \langle\sigma v\rangle_{n,exc}(r) + n_{Ar^{17+}}(r) \langle\sigma v\rangle_{n,rr}(r) \right] + n_o(r)\, n_{Ar^{17+}}(r) \langle\sigma v\rangle_{n,cx} (r) \qquad (1)$$

where n_o (r) is the neutral hydrogen density and the subscripts ex, rr and cx denote excitation, radiative recombination and charge transfer recombination. Radiative transitions to any levels except the ground state, collisional de-excitation and excitation from any other levels, ionization, cascades from upper levels, and dielectronic recombination have all been ignored. Excitation and radiative recombination rates have been taken from Ref. 23, and charge exchange cross-sections for fully stripped chlorine (to model hydrogen-like argon) have been interpolated from Ref. 31. Density profiles for hydrogen- and helium-like argon have again been determined from the code modelling, including the effects of anomalous impurity transport. Shown in Fig. 13 are the calculated emissivity profiles for 1s3p - $1s^2$ to 1s12p - $1s^2$ transitions, demonstrating the individual effects of excitation (a), radiative recombination (b) and charge exchange recombination (c), in addition to the composite profiles of excitation and radiative recombination (d) and the grand total (e). Plasma parameters for these calculations were T_{eo} = 1800 eV, a_T = 10 cm, $n_{eo} = 2.2 \times 10^{14} cm^{-3}$, a_L = 16.5 cm, α = 0.5, $T_i = .8\, T_e$ and $n_o = 5 \times 10^6 cm^{-3}$ $[1 + .00347 \exp (.815\, r\, (cm))]$. It is apparent that collisional excitation is most important inside of 10 cm while radiative recombination dominates between 10 cm and the limiter radius for most of the lines. Charge transfer recombination is only important for the n = 8, 9 and 10 levels at the outer radii although it may contribute to lower n levels following subsequent cascades. It has been assumed that 25% of the charge transfer occurs into the p levels[33], ℓ mixing[34] has been ignored and it has been assumed that 1/4 of the charge transfer occurs into singlet levels, the states which primarily give rise to observed x-rays. These factors have been included in $\langle \sigma v \rangle_{n,cx}$ in Eq. 1.

Brightness profiles for these conditions, obtained from the calculated emissivity profiles, assuming an instrumental spatial resolution of 3 cm, are shown in Fig. 14. These calculated brightness profiles are in good agreement with observations, demonstrated in Fig. 12. Emissivity profiles obtained from abel inversion of the observed brightness profiles, along with calculated profiles, can be found in Ref. 16. In Fig. 15 are shown the radial profiles of the ratios of brightnesses of 1snp - $1s^2$ transitions to the 1s7p - $1s^2$ line for n = 8,9,10 and 11. The enhancement for n = 9 and n = 10 becomes very apparent beyond 8 cm. This enhancement, which is attributed entirely to charge exchange recombination, may be used to calculate the neutral density profile.

VII. Neutral density profiles

Since the spectrometer system does not have an absolute intensity calibration and since the absolute argon density in the plasma is not directly measured, the product of these two factors can be determined by comparison of the observed relative emissivity of a particular line, e_n (r), and the calculated emissivity from Eq.1, E_n (r). For the central emissivity of the 1s7p - $1s^2$ line, for example, charge exchange recombination is negligible, and the relative emissivity is

$$e_7(0) = A\, n_e(0) \left[\langle \sigma v \rangle_{7,exc}(0) + n_{Ar^{17+}}(0)/n_{Ar^{16+}}(0) \langle \sigma v \rangle_{7,rr}(0) \right] \quad (2)$$

where A is the normalization constant. The cross sections are known functions of electron temperature, the electron density is measured, the ratio of hydrogen- to helium-like argon densities is determined from the transport code and the central relative emissivity is obtained from Abel inversion of the observed brightness profile of the 1s7p - 1s^2 line. This determines the normalization constant, A. The neutral hydrogen density profile can then be determined from Eq. 1 using a transition for which charge exchange recombination is important. For the 1s9p - 1s^2 line, for example, the neutral density may be found from

$$n_o(r) = \frac{e_9(r)/A - n_e(r)\left(\langle \sigma v \rangle_{9,exc}(r) + n_{Ar^{17+}}(r)/n_{Ar^{16+}}(r) \langle \sigma v \rangle_{9,rr}(r)\right)}{\langle \sigma v \rangle_{9,cx}(r)\, n_{Ar^{17+}}(r)/n_{Ar^{16+}}(r)} \quad (3$$

An example of a neutral density profile determined in this fashion from the 1s9p - 1s^2 and 1s10p - 1s^2 emissivities is shown in Fig. 16. The inferred neutral density increases two orders of magnitude in going from $2 \times 10^7 cm^{-3}$ at 9 cm to $2 \times 10^9 cm^{-3}$ at 14 cm. Also plotted are neutral density profiles calculated from the FRANTIC neutral transport code[35]. The agreement is quite good although there are several uncertainties in both the calculations and measurements. These measurements were obtained at a limiter port, which may have a different neutral density than at other toroidal locations[36]. There are also known to be poloidal asymmetries in edge conditions[37] which can affect conclusions about the neutral density profile. Another source of uncertainty in these neutral density profile estimates is that values of the Ar^{17+} to Ar^{16+} ratios were obtained from the results of the impurity transport code simulations.

VIII. Very High n Transitions in Ar^{16+}

The concern of Section V was the effect of charge transfer recombination between Ar^{17+} and neutral hydrogen in the ground state. As was shown, there is a large enhancement at the plasma edge of the 1s9p - and 1s10p-$1s^2$ transitions in Ar^{16+}. At slightly shorter wavelengths there is an even larger manifestation[16] of charge exchange recombination, as shown in Fig.17. This is a spectrum in the vicinity of the ionization limit of Ar^{16-} obtained from the plasma periphery for a series of 80 kG, hydrogen discharges with $\bar{n}_e = 1.8 \times 10^{14}$ cm^{-3} and $T_{eo} = 1800$ eV. There is a broad emission feature between 3009 and 3020 mÅ which has a maximum at 3013 mÅ and a shoulder at 3017 mÅ. The series limit is at 3008.8 mÅ. The peak and the shoulder occur near the wavelengths for the 1s27p - $1s^2$ and 1s18p - $1s^2$ transitions, respectively, in Ar^{16+}. These are integral multiples of n = 9, the level into which charge transfer occurs from neutral hydrogen in the ground state. The upper levels of these lines are populated by charge transfer from neutral hydrogen in the excited n = 3 and n = 2 levels[38], respectively. The radial brightness profile of this feature is included in Fig. 12 and the maximum emission emanates from the plasma edge, near r = 13 cm, indicating that this feature is populated by a recombination process.

IX. Satellite Lines and Radial Profiles

In Section IV and VI were presented radial brightness profiles of ground state transitions in helium-like argon. Close in wavelength to these transitions are satellites due to lithium- and beryllium-like argon. Radial profiles of the satellites tend to be broader than the corresponding helium-like profiles because at least some of the upper levels are formed by dielectronic recombination which has a weaker temperature dependence than collisional excitation. Radial brightness profiles of the satellites to the n = 2 upper level spectra are shown in Fig. 18. Li indicates the sum of all lines between 3.975 and 3.987 Å (q, r, and a), m corresponds to the n = 3 spectator transitions between 3.953 and 3.957 Å, and Be is due to all lines between 4.007 and 4.023 Å. The satellite profiles are all relatively flat near the plasma center and then fall off extremely rapidly outside of 9 cm.

The satellites to the n > 3 ground state transitions exhibit similar behavior. Shown in Fig. 19 are spectra in the wavelength region from 3.13 to 3.22 Å from three discharges with a_L = 16.5 cm. Wavelengths and line identifications are given in Table II and will be discussed in detail in a forthcoming paper[29]. About halfway out in minor radius (8.5cm) the satellites have grown significantly with respect to the 1s4p and 1s5p-$1s^2$ transitions. [The satellites in this region are mainly due to n = 2 spectator electrons perturbing the 1s5p- and 1s6p -$1s^2$ transitions]. The satellites all abruptly disappear at slightly larger minor radius. Shown in Fig. 20 are radial profiles of the brightness ratios of the satellite lines to the 1s4p-$1s^2$ transition. These curves have a strong maximum at 8.5 cm, which depends on the particular temperature profile shape for given operating conditions.

X. Conclusions

Spectra and radial brightness profiles of all the ground state transitions in helium-like argon have been obtained. Modelling of the line intensities of Δ n = 1 ground state transitions indicates that for the plasma center, electron impact excitation is the strongest population process for the upper levels. In the cooler outer regions of the plasma, radiative recombination of hydrogen-like argon is very important for populating the upper levels in Ar^{16+}. Fast impurity transport from the plasma center is crucial in providing sufficient Ar^{17+} in the cooler regions for the recombination to occur. Near the limiter radius, there is an excess of emission in the triplet lines over that expected from the line intensity model. This is possibly due to the improper treatment of cascades from upper levels in helium-like argon, which themselves have been populated by radiative and charge transfer recombination. Radial profiles of $\Delta n > 1$ ground state transitions have also been measured and similar to the $\Delta n = 1$ transitions, excitation is most important in populating the upper levels near the plasma center, while radiative recombination dominates at the edge. For the transitions 1s9p - and 1s10p - $1s^2$, charge exchange recombination from instrinsic neutral hydrogen is by far the most important population process near the plasma edge. The intensities of these lines have been used to deduce neutral hydrogen density profiles. High n transitions ($1snp-1s^2$, with $13<n<40$) have been observed to be populated solely by charge transfer between excited neutral hydrogen and Ar^{17+}.

XI. Acknowledgements

Operation of Alcator C by D. Gwinn and B. Lipschultz is gratefully acknowledged. Calculations by C. Fiore and V. Safranova, data reduction by M. Ono and support from R. Parker are also appreciated. Work supported by Department of Energy Contract # DE-AC02-78ET51013.

XII. References

1 M. Bitter et al., Phys. Rev. Lett. 42, 304 (1979).

2 M. Bitter et al., Phys. Rev. Lett. 43, 129 (1979).

3 M. Bitter et al., Phys. Rev. Lett. 47, 921 (1981).

4 E. Källne et al., Phys. Rev. Lett. 49, 330 (1982).

5 F. Bely-Dubau et al., Phys. Rev. A 26, 3459 (1982).

6 E. Källne et al., Phys. Rev. A 27, 2682 (1983).

7 E. Källne et al., Phys. Rev. A 28, 467 (1983).

8 E. Källne et al., Phys. Rev. Lett. 52, 2245 (1984).

9 M. Bitter et al., Phys. Rev. A 29, 661 (1984).

10 P. Lee et al., Phys. Rev. A 31, 3996 (1985).

11 P. Lee et al., Phys. Rev. Lett. 55, 386 (1985).

12 TFR Group et al., Phys. Rev. A 32, 2374 (1985).

13 M. Bitter et al., Phys. Rev. A 32, 3011 (1985).

14 E. Källne et al., Nucl. Instrum. Meth. Phys. Res. B9, 698 (1985).

15 E. Källne et al., Physica Scripta 31, 551 (1985).

16 J. E. Rice et al., Phys. Rev. Lett. 56, 50 (1986).

17 E. S. Marmar et al., Phys. Rev. A 33, 774 (1986).

18 B. Blackwell et al., in Plasma Physics and Controlled Nuclear Fusion Research 1982 Vol.II, 27 (1982).

19 J. Källne et al., Nucl. Instrum. Meth. 203, 415 (1982).

20 L. A. Vainshtein and U. I. Safranova, Atomic Nuclear Data Tables 21, 49 (1982) and 25, 311 (1982).

21 C. P. Bhalla and T. W. Tunnel, J. Quant. Spectrosc. Rad. Trans. 32, 141 (1984).

22 R. Mewe and J. Schrijver, Astron. Astroph. 65, 99 (1978).

23 R. C. Isler, Nucl. Fusion 24, 1599 (1984).

24 E. S. Marmar et al, Nucl. Fus. 22, 1567 (1982).

25 A. Pradhan, Ap. J. 288, 824 (1985).

26 J. F. Seely and U. Feldman, Phys. Rev. Lett. 54, 1016 (1985).

27 P. G. Burkhalter et al., J. Appl. Phys. 50, 532 (1979).

28 U. I. Safranova, Private communication (1985).

29 E. Källne et al., to be published.

30 W. L. Wiese, M. W. Smith and B. M. Glennon, Atomic Transition Probabilities NSRDS-NBS 4, (1966).

31 R. K. Janev, D. S. Belic and B. H. Bransden, Phys. Rev. A 28, 1293 (1983).

32 R. C. Isler and E. C. Crume, Phys. Rev. Lett. 41, 1296 (1978).

33 V. A. Abramov, F. F. Baryshnikov and V. S. Lisitsa, JETP Lett., 27, 465 (1978).

34 R. Fonck et al., Phys. Rev. A 29, 3288 (1984).

35 C. L. Fiore, private communication (1985).

36 E. S. Marmar, J. Nucl. Mat. 76 and 77, 59 (1978).

37 B. Lipschultz et al., Nucl. Fus. 24, 977 (1985).

38 R. Olson, J. Phys. B. 13, 483 (1980).

Table 1

Name	Transition	Rel. Int.	λ	λ_{VS}	λ_{BT}	λ_{TFR}
	$1s2p3d\ ^2P_{3/2} - 1s^23d\ ^2D_{5/2}$?	.026	3.9454	3.9449		
w	$1s2p\ ^1P_1 - 1s^2\ ^1S_0$	1.000	3.9482	3.9482		3.9451
	$1s2p3d\ ^2F_{7/2} - 1s^23d\ ^2D_{5/2}$?	.087	3.9510	3.9498		3.9458
	$1s2p3p\ ^2D_{5/2} - 1s^23p\ ^2P_{1/2}$?	.032	3.9537	3.9543		
	$1s2p3p\ ^2D_{5/2} - 1s^23p\ ^2P_{3/2}$	.072	3.9553	3.9553		
	$1s2p^2\ ^2S_{1/2} - 1s^22p\ ^2P_{1/2}$?	.009	3.9615	3.9611		
x	$1s2p\ ^3P_2 - 1s^2\ ^1S_0$	.207	3.9649	3.9649		3.9622
y	$1s2p\ ^2P_1 - 1s^2\ ^1S_0$	.269	3.9682	3.9683		3.9659
q	$1s2s2p\ ^2P_{3/2} - 1s^22s\ ^2S_{1/2}$	.059	3.9806	3.9806	3.9785	3.9777
	$1s2p^2\ ^2P_{3/2} - 1s^22p\ ^2P_{1/2}$	----		3.9811		
r	$1s2s2p\ ^2P_{1/2} - 1s^22s\ ^2S_{1/2}$	.051	3.9830	3.9827	3.9807	3.9801
a	$1s2p^2\ ^2P_{3/2} - 1s^22p\ ^2P_{3/2}$	.018	3.9855	3.9852	3.9826	3.9823
k	$1s2p^2\ ^2D_{3/2} - 1s^22p\ ^2P_{1/2}$	.096	3.9894	3.9892	3.9865	3.9866
j	$1s2p^2\ ^2D_{5/2} - 1s^22p\ ^2P_{3/2}$	----		3.9932	3.9898	3.9907
z	$1s2s\ ^3S_1 - 1s^2\ ^1S_0$	.561	3.9934	3.9934		3.9909

Table 2

Name	Transition	Rel. Int.	λ	λ_S	λ_{BSFC}
Ar^{16+}	$1s3p - 1s^2$		3.3654		
sat	$1s^2p4p-1s^22p$	.145	3.2728	3.2722	
sat	$1s2p4p-1s^22p$	.310	3.2713	3.2709	3.270
sat	$1s2s4p-1s^22s$	.083	3.2622	3.2629	3.259
sat		.011	3.2469		
sat	$1s2s4p-1s^22p$	.032	3.2454	3.2458	3.245
sat	$1s2p5p-1s^22p$	.182	3.2046	3.2049	3.202
Ar^{16+}	$1s4p - 1s^2$	1.000	3.1999		
sat	$1s2s5p-1s^22p$	.050	3.1947	3.1949	3.192
sat		.020	3.1784		
sat	$1s2p6p-1s^22p$	.077	3.1693	3.1696	3.167
sat	$1s2s6p-1s^22s$	.034	3.1590	3.1594	3.156
Ar^{17+}	$3p-1s$	.096	3.1510		
sat	$1s2p7p-1s^22p$	.065	3.1491		3.146
sat		.008	3.1429	3.1433	
Mo?		.027	3.1382		
sat		.038	3.1349		
Ar^{16+}	$1s5p - 1s^2$	.449	3.1285		

XIII. Figure Captions

1. Spectrum of $\Delta n = 1$ ground state transitions of helium-like argon in the wavelength region from 3.94 to 4.02 Å a). on a linear scale and b). on a logarithmic scale including fit.

2. Spectra of helium-like argon at four different radial locations. Local electron temperatures for the four cases are 1650 eV, 550 eV, 250 eV and 100 eV. The vertical scales are all arbitrary.

3. Observed radial brightness profiles for different components of the helium-like argon spectrum.

4. Density profiles of the different charge states of argon a.) assuming coronal equilibrium and b.) including anomalous impurity transport.

5. Calculated brightness profiles for the coronal equilibrium density profiles a). with collisional excitation as the only population mechanism and b.) including excitation and recombination.

6. Calculated brightness profiles for the anomalous impurity transport density profiles a.) for excitation only and b.) including recombination.

7. Observed brightness profiles and b.) calculated profiles including transport, excitation and recombination enhanced by a factor of five.

8. Observations of $1snp-1s^2$ transitions in Ar^{16+} for $3 < n < 12$ in the wavelength region from 3.0 to 3.4 Å.

9. The intensities of the central chord 1snp-1s2 lines as a function of n, compared to the oscillator strengths.

10. Spectra from $1s7p-1s^2$ to $1s11p-1s^2$ transitions from three radial locations.

11. Spectra from $1s8p - 1s^2$ to $1s13p - 1s^2$ transitions from two different chords obtained in a.) helium working gas and b.) hydrogen working gas.

12. Observed brightness profiles of $1snp-1s^2$ transitions in Ar^{16+}.

13. Calculated emissivity profiles for $1snp-1s^2$ transitions of Ar^{16+} assuming the upper levels were populated by a.) collisional excitation, b.) radiative recombination, c.) charge exchange recombination, d.) collisional excitation and radiative recombination, and e.) the grand composite of a.), b.), and c.).

14. Calculated brightness profiles from Fig. 13e.

15. Radial profiles of the ratios of $1snp-1s^2$ to $1s7p-1s^2$ with n = 8,9,10 and 11.

16. Neutral hydrogen density profiles obtained from the charge transfer enhancements of the $1s9p-1s^2$, $1s10p-1s^2$ and very high n transitions over the calculated values from population by excitation and radiative recombination. FRANTIC code calculations are shown for comparison.

17. Spectrum from transitions of very high n levels to the ground state in the vicinity of the ionization limit of Ar^{16+}.

18. Radial profiles of satellites to n = 2 to n = 1 transitions.

19. Spectra of satellites in the vicinity of the 1s4p and $1s5p-1s^2$ lines for three radial locations.

20. Radial profiles of the brightness ratios of satellites and the $1s4p-1s^2$ transitions.

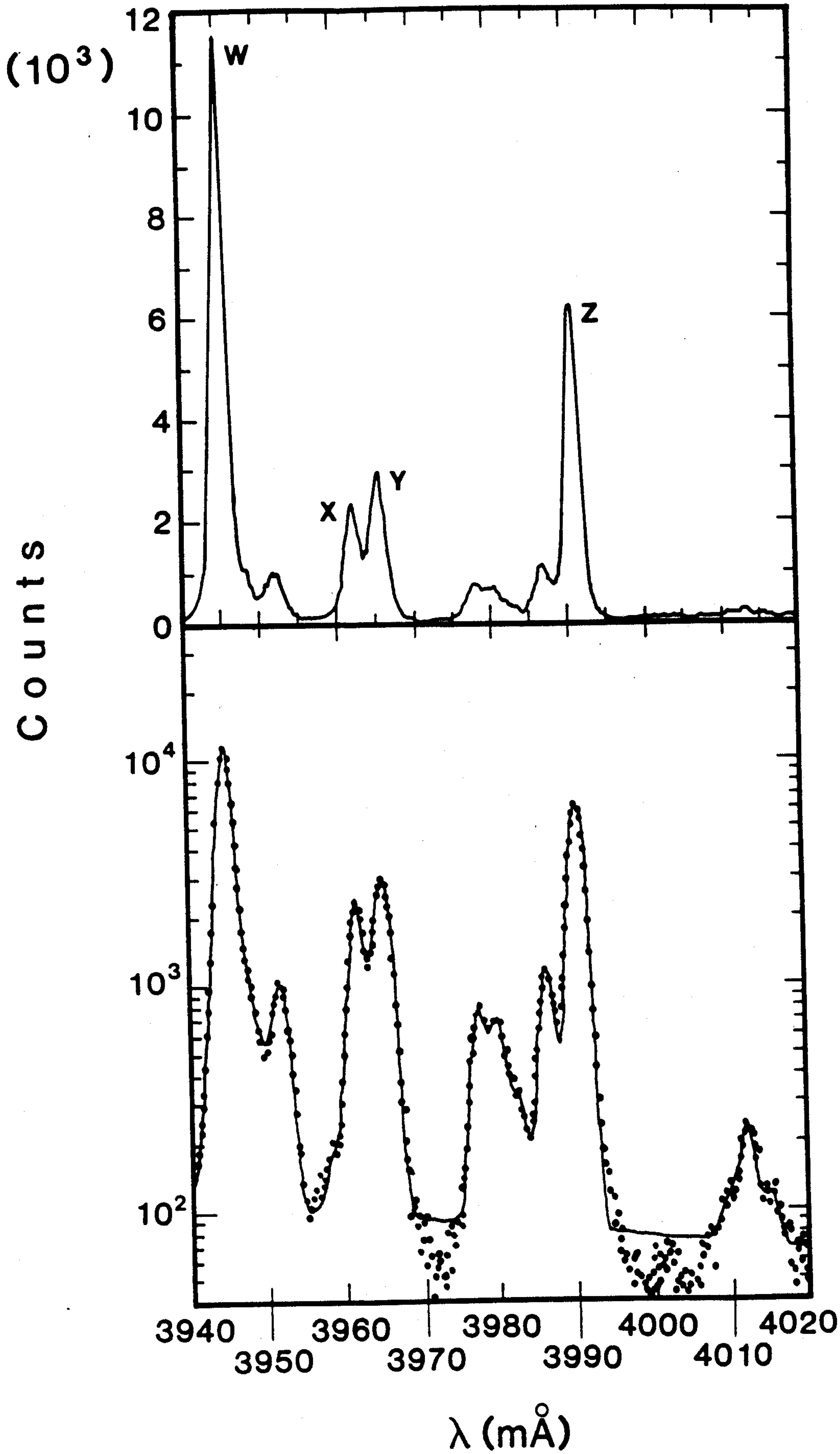

12
(10³)
10
8
6
4
2
0
W
X
Y
Z
Counts
10⁴
10³
10²
3940
3950
3960
3970
3980
3990
4000
4010
4020
λ (mÅ)

Figure 1

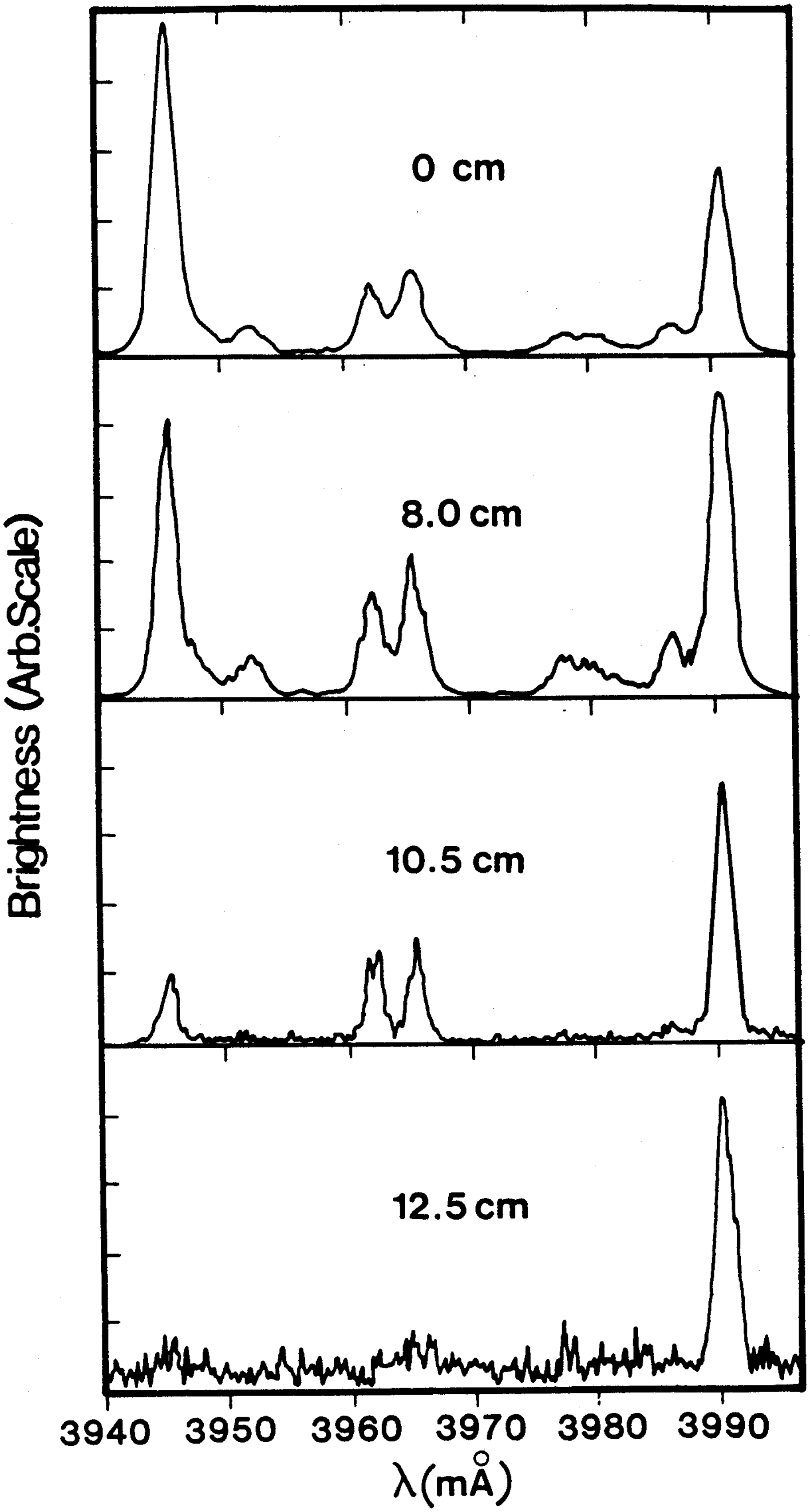
0 cm
8.0 cm
10.5 cm
12.5 cm
Brightness (Arb.Scale)
3940
3950
3960
3970
3980
3990
λ(mÅ)

Figure 2

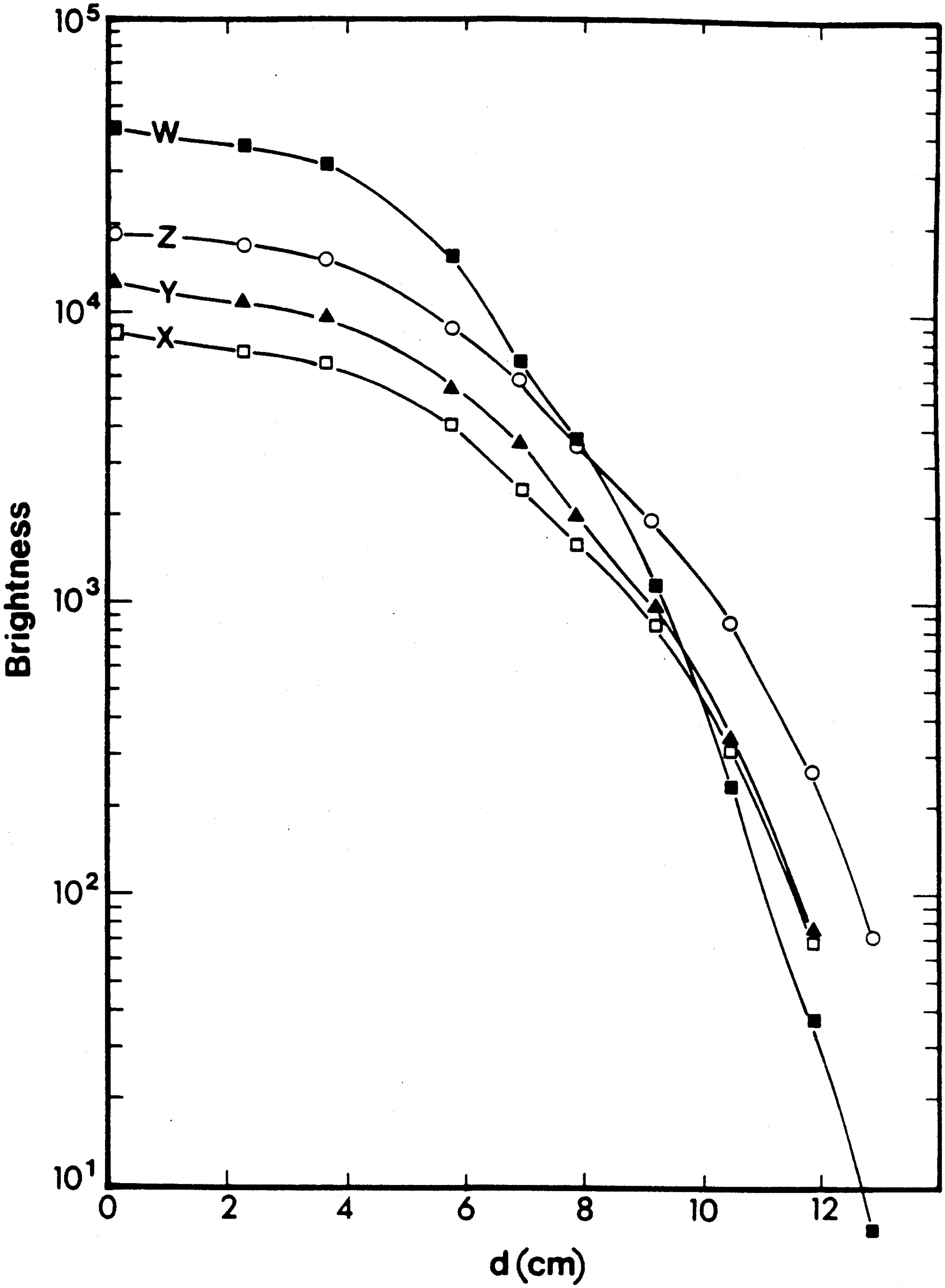

Figure 3

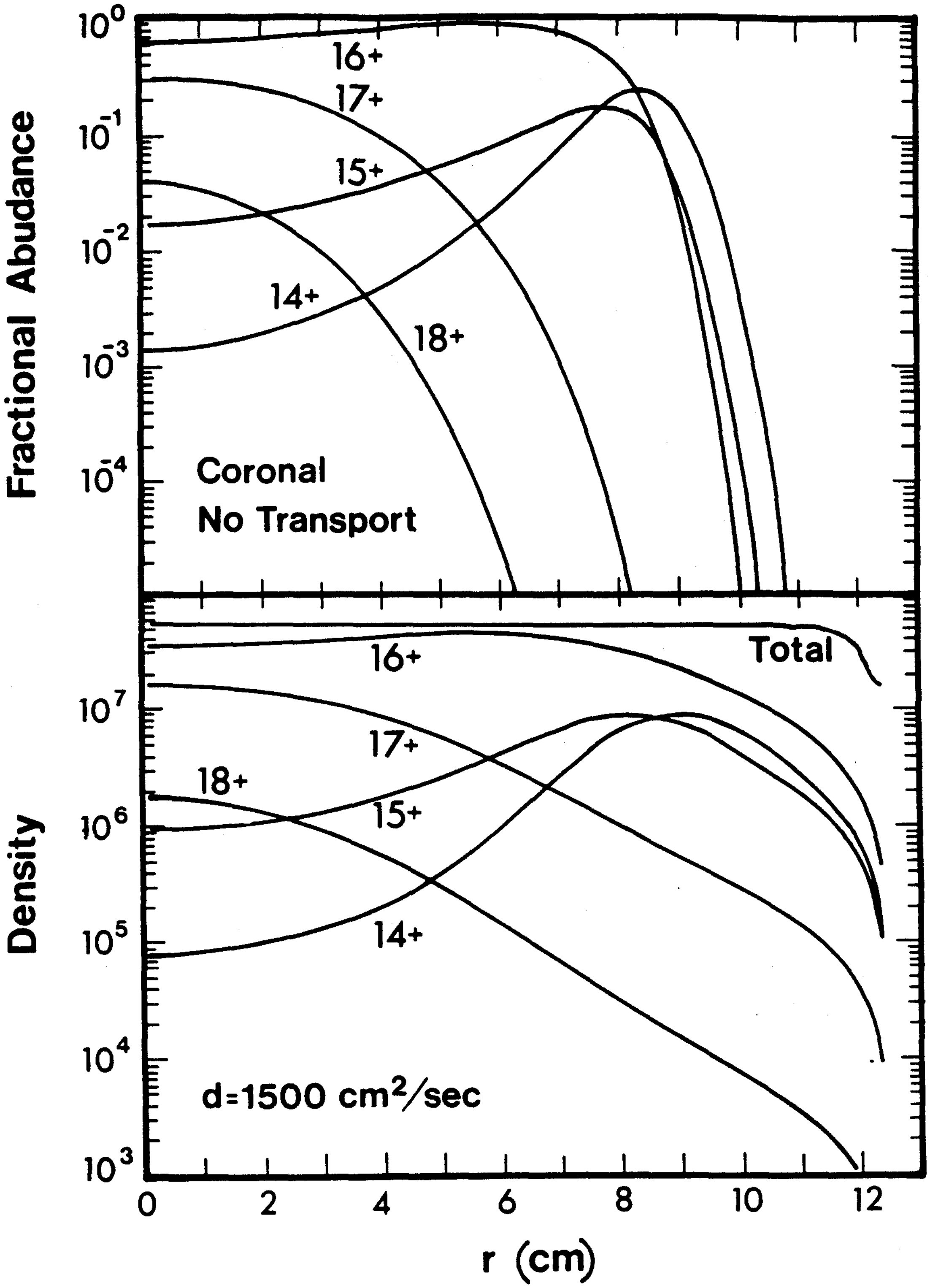

Fractional Abudance
Density
Coronal
No Transport
d=1500 cm²/sec
Total
14+
15+
16+
17+
18+
r (cm)
0
2
4
6
8
10
12

Figure 4

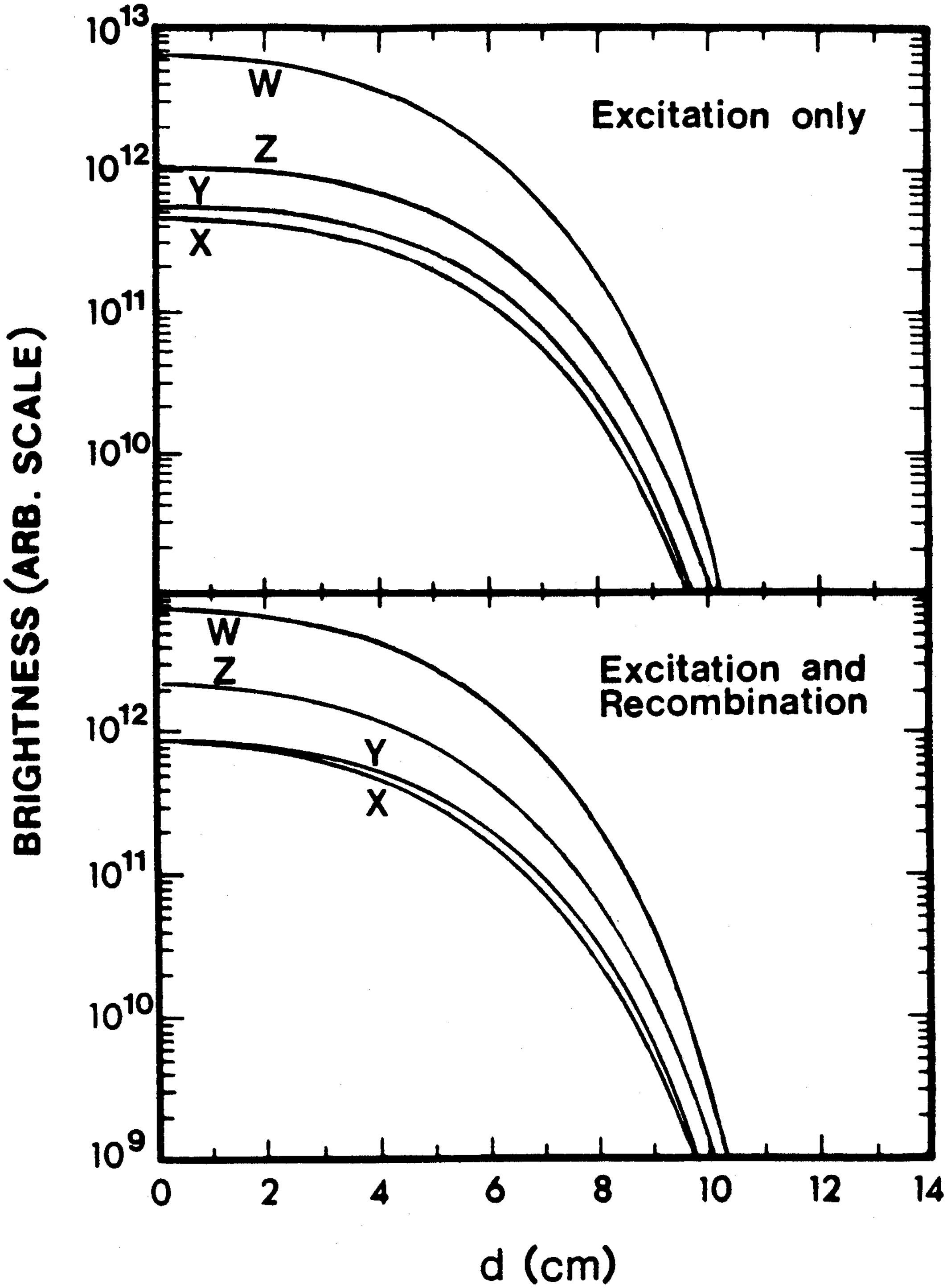

Excitation only
Excitation and Recombination
W
Z
Y
X
BRIGHTNESS (ARB. SCALE)
d (cm)
10^{13}
10^{12}
10^{11}
10^{10}
10^{9}
0
2
4
6
8
10
12
14

Figure 5

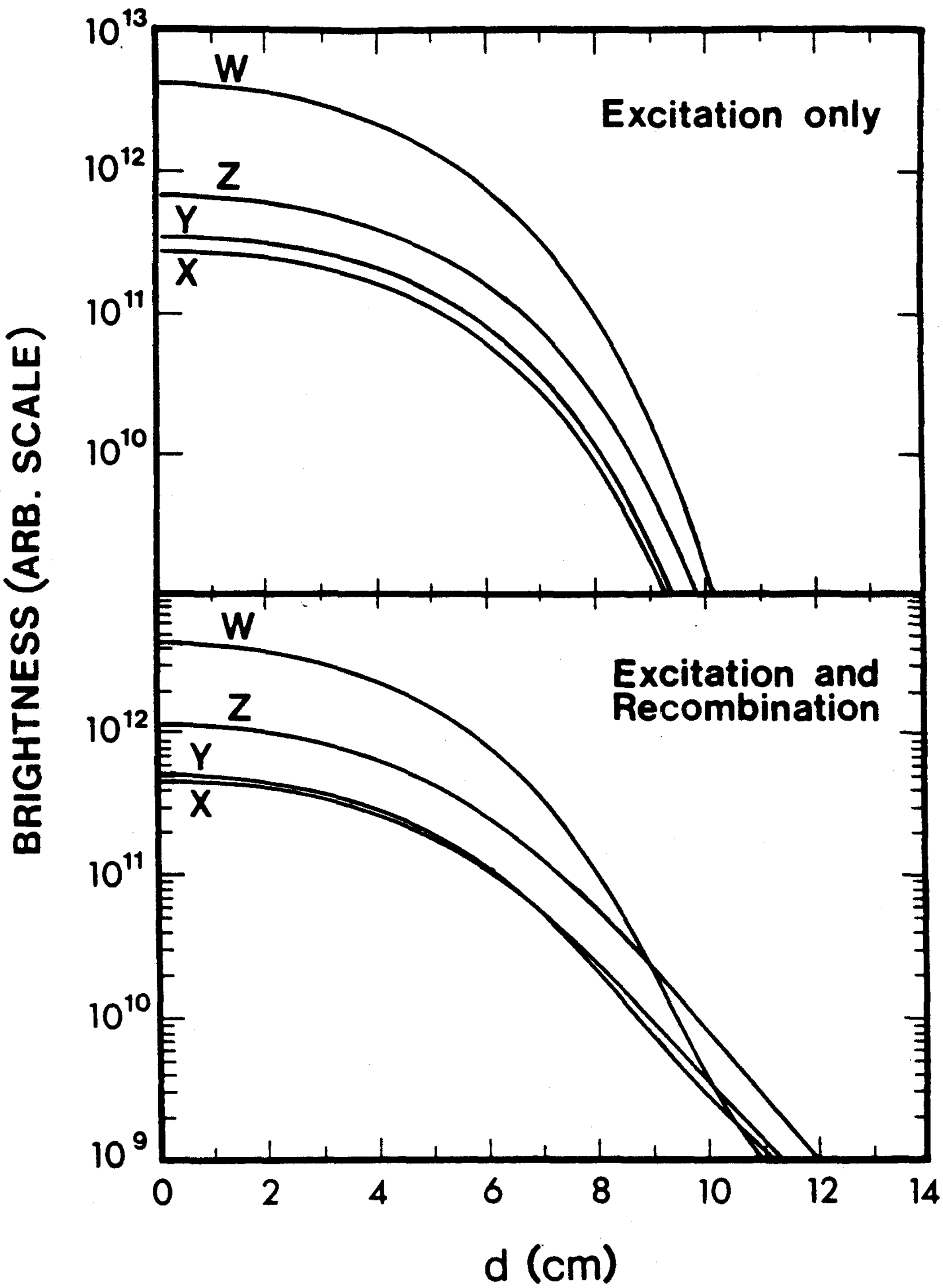
BRIGHTNESS (ARB. SCALE)
10^{13}
10^{12}
10^{11}
10^{10}
10^{9}
W
Z
Y
X
Excitation only
Excitation and Recombination
0
2
4
6
8
10
12
14
d (cm)

Figure 6

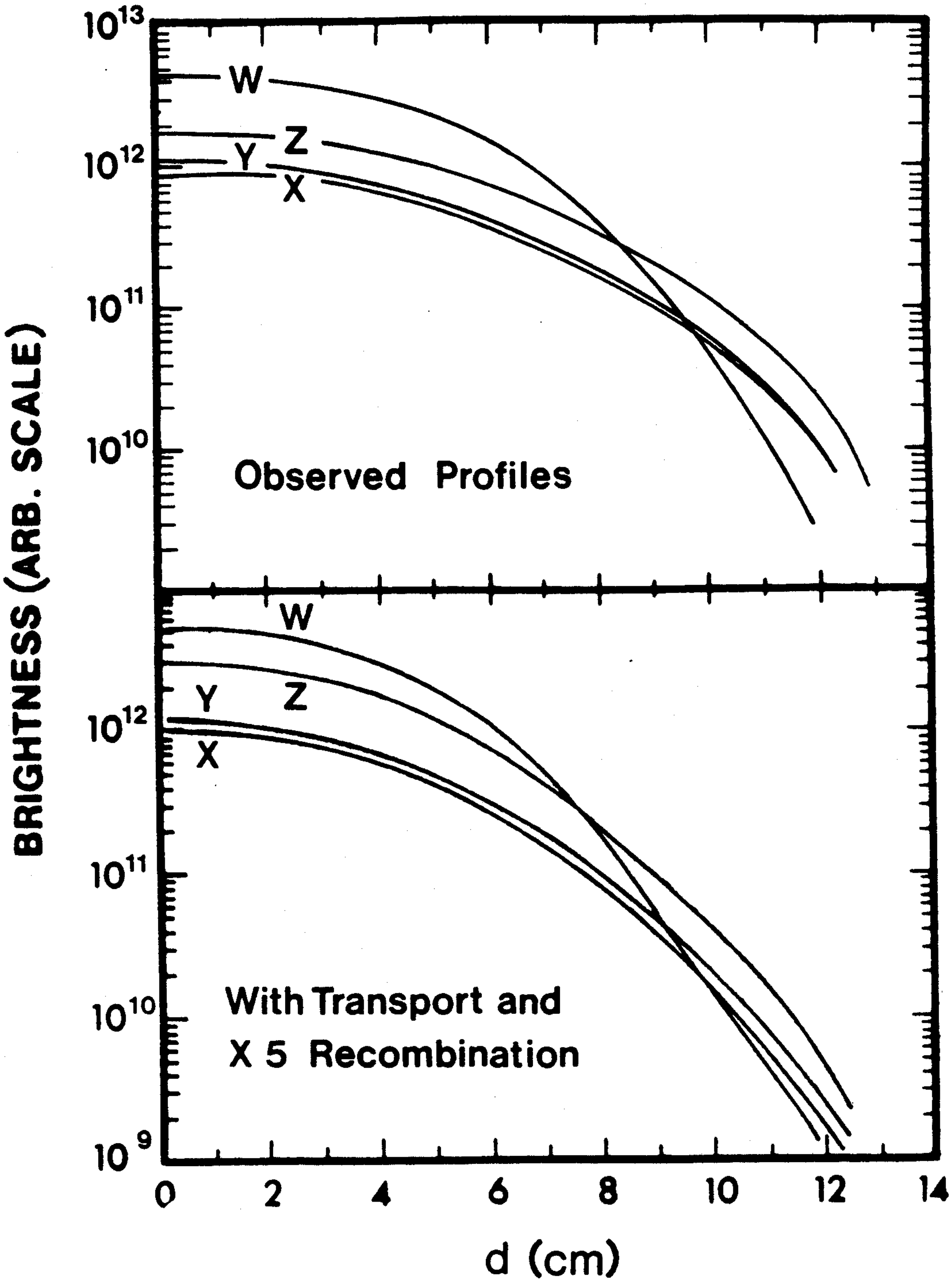
BRIGHTNESS (ARB. SCALE)
W
Z
Y
X
Observed Profiles
With Transport and
X 5 Recombination
10^{13}
10^{12}
10^{11}
10^{10}
10^{9}
0
2
4
6
8
10
12
14
d (cm)

Figure 7

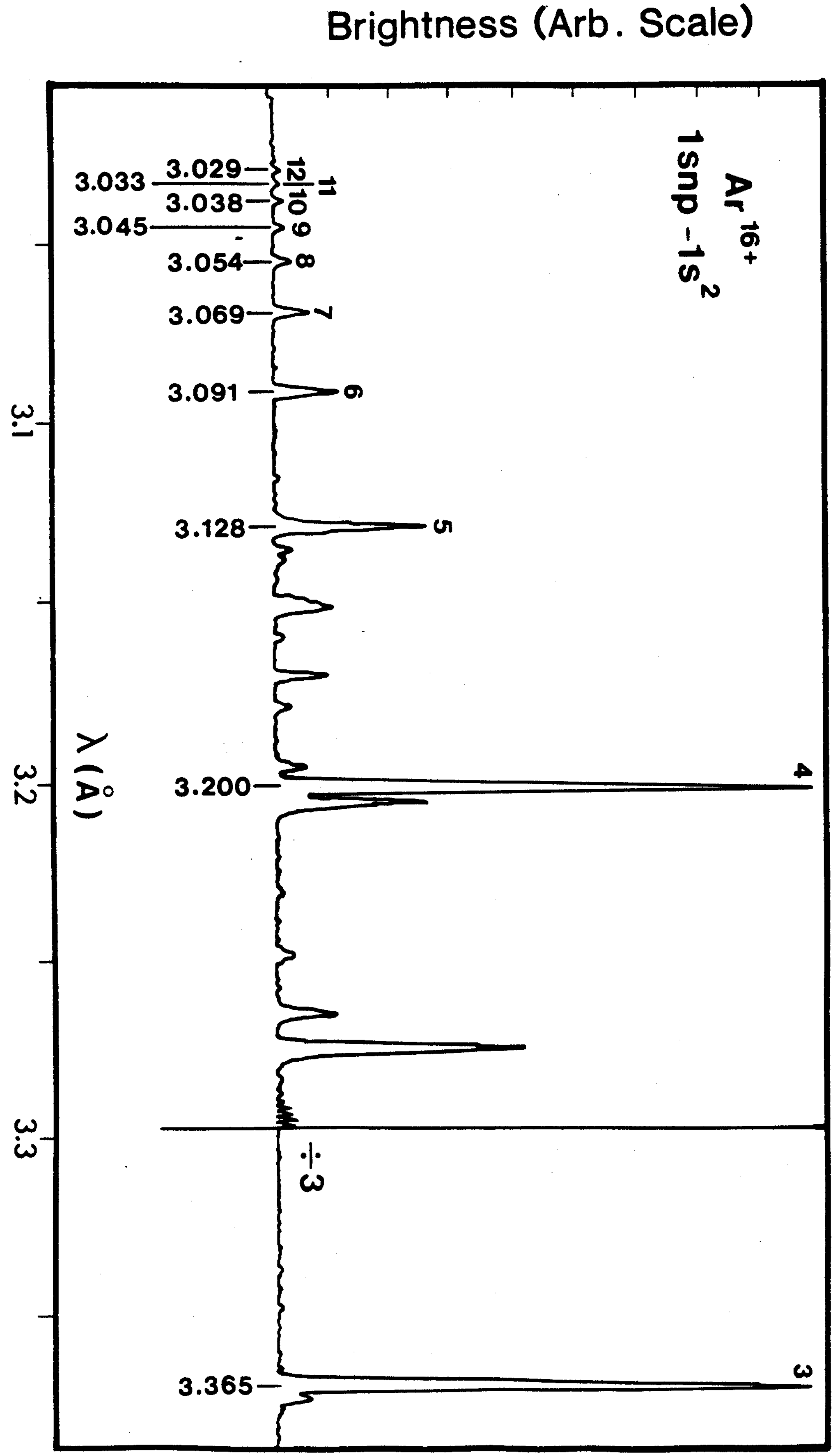

Brightness (Arb. Scale)
Ar 16+
1snp -1s2
λ (Å)
3.1
3.2
3.3
3.029
3.033
3.038
3.045
3.054
3.069
3.091
3.128
3.200
3.365
12
11
10
9
8
7
6
5
4
3
÷3

Figure 8

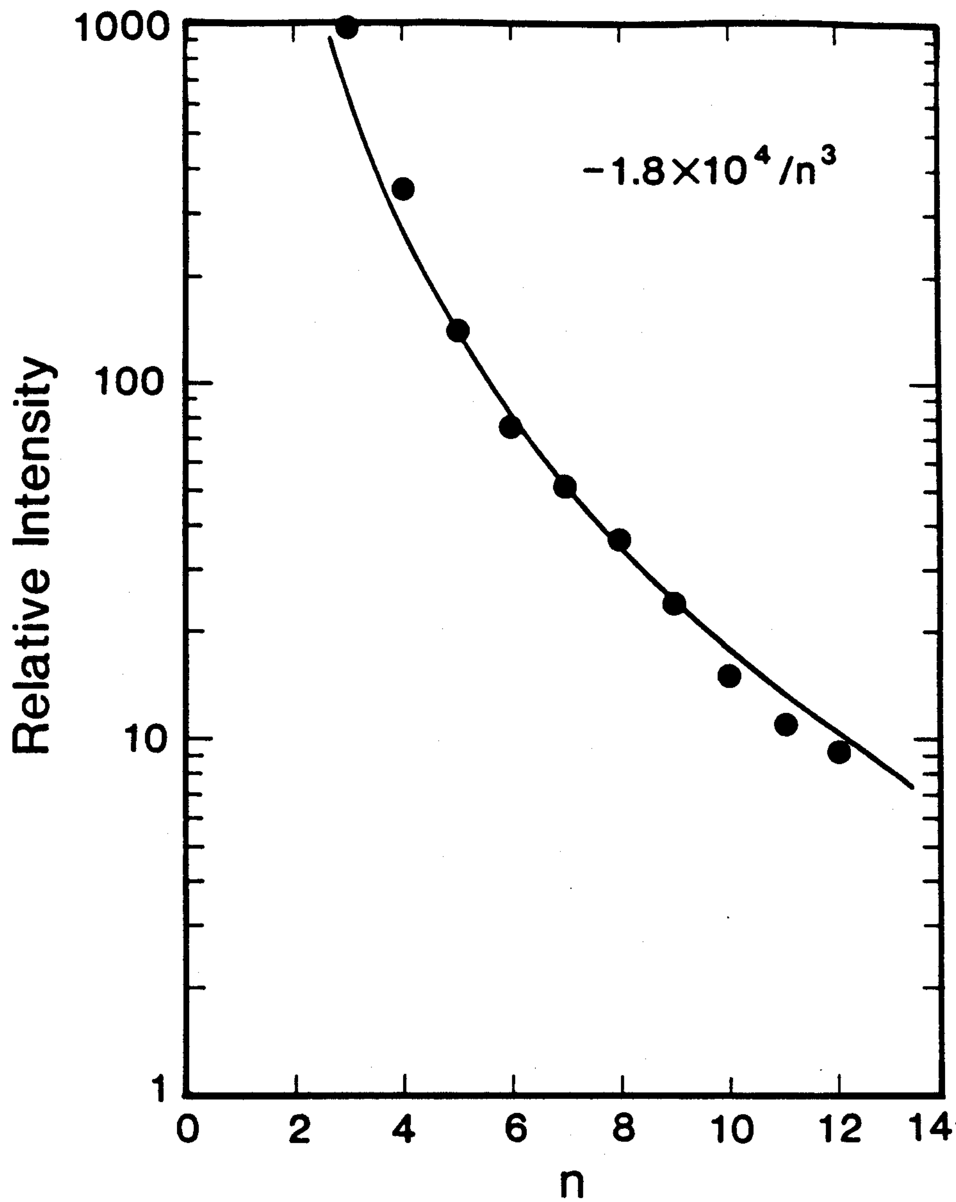
1000
100
10
1
0
2
4
6
8
10
12
14
Relative Intensity
n
$-1.8\times10^4/n^3$

Figure 9

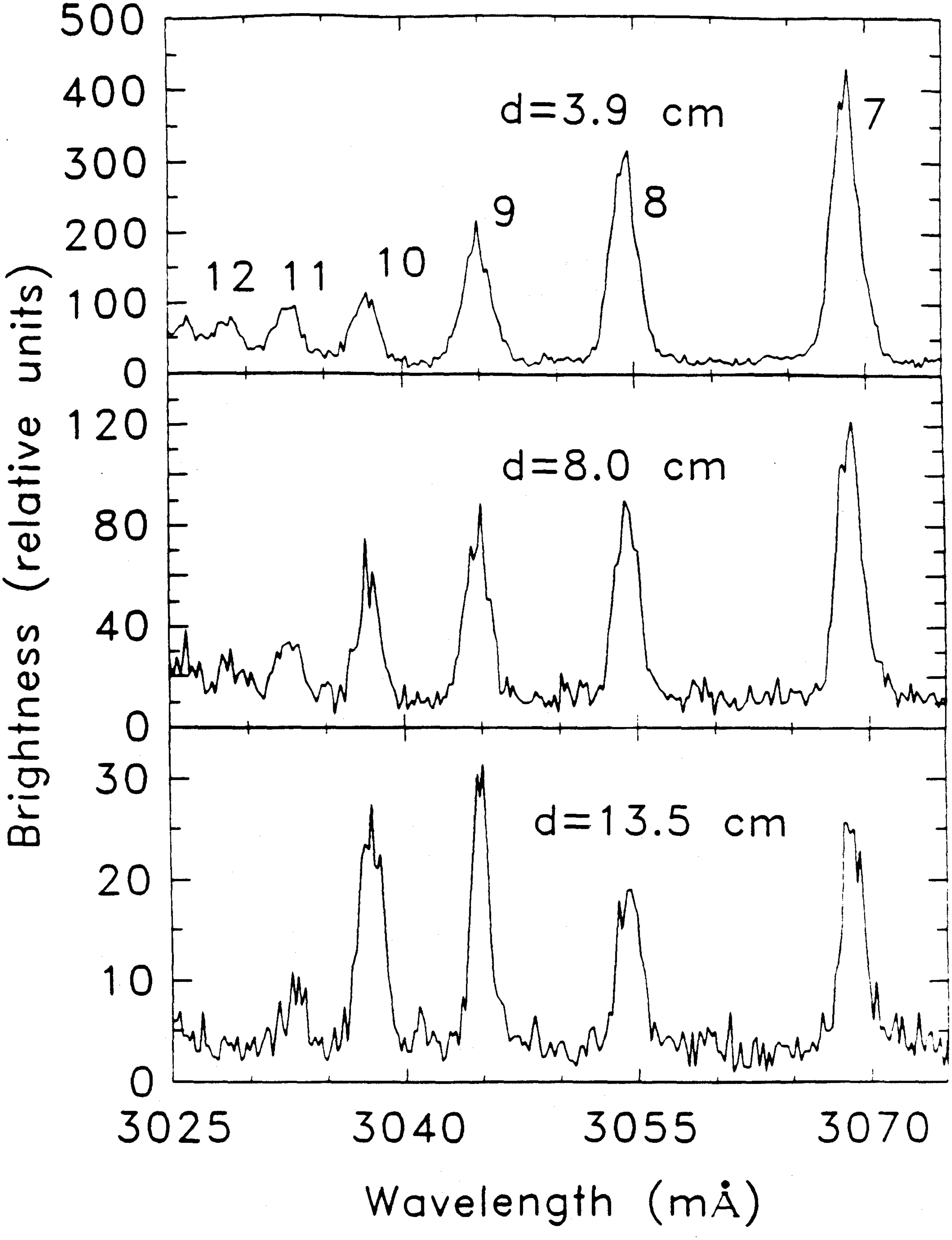
d=3.9 cm
7
8
9
10
12
11
d=8.0 cm
d=13.5 cm
500
400
300
200
100
0
120
80
40
0
30
20
10
0
Brightness (relative units)
3025
3040
3055
3070
Wavelength (mÅ)

Figure 10

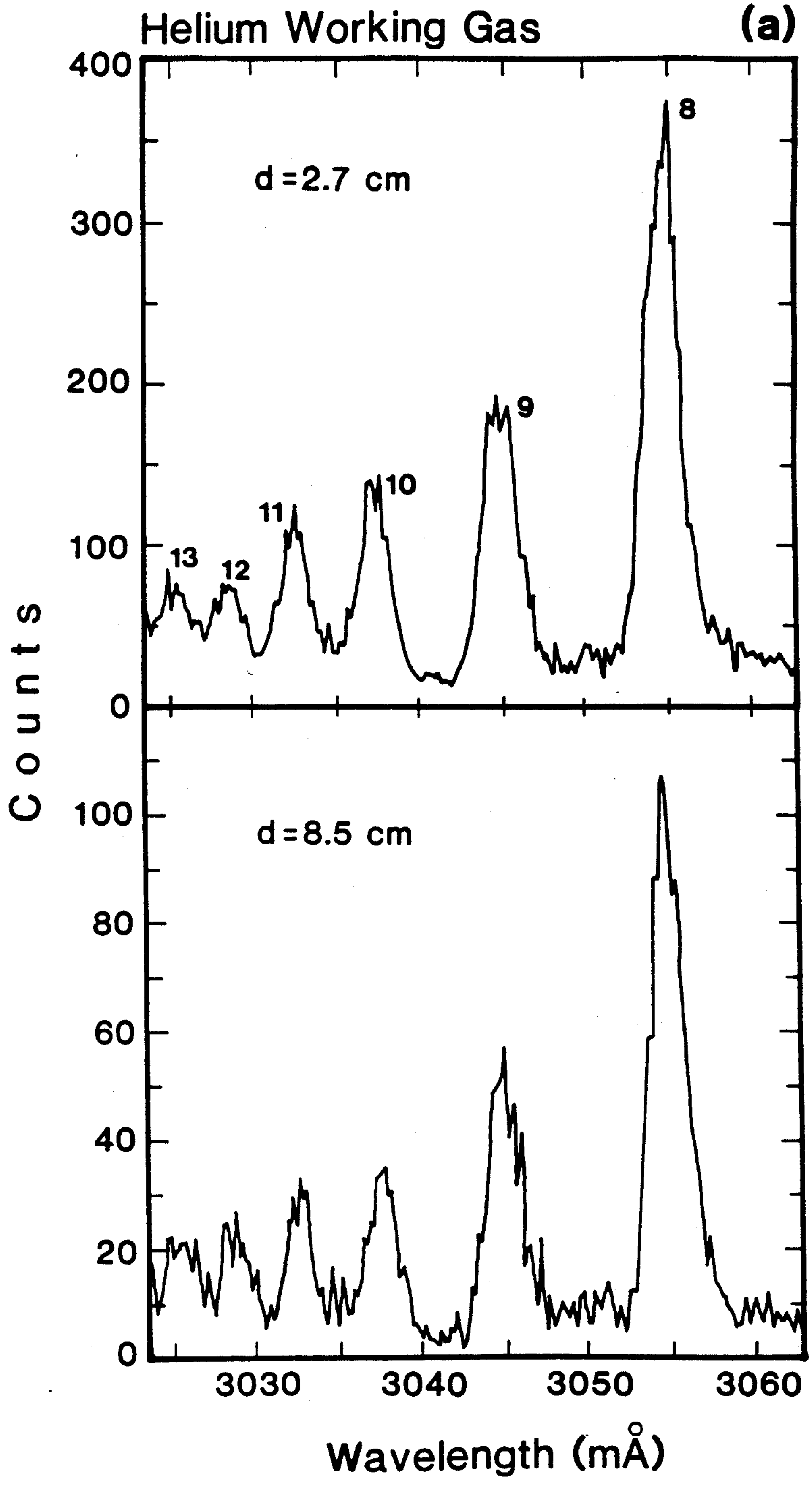

Helium Working Gas
(a)
400
300
200
100
0
d=2.7 cm
8
9
10
11
12
13
Counts
100
80
60
40
20
0
d=8.5 cm
3030
3040
3050
3060
Wavelength (mÅ)

Figure 11 (a)

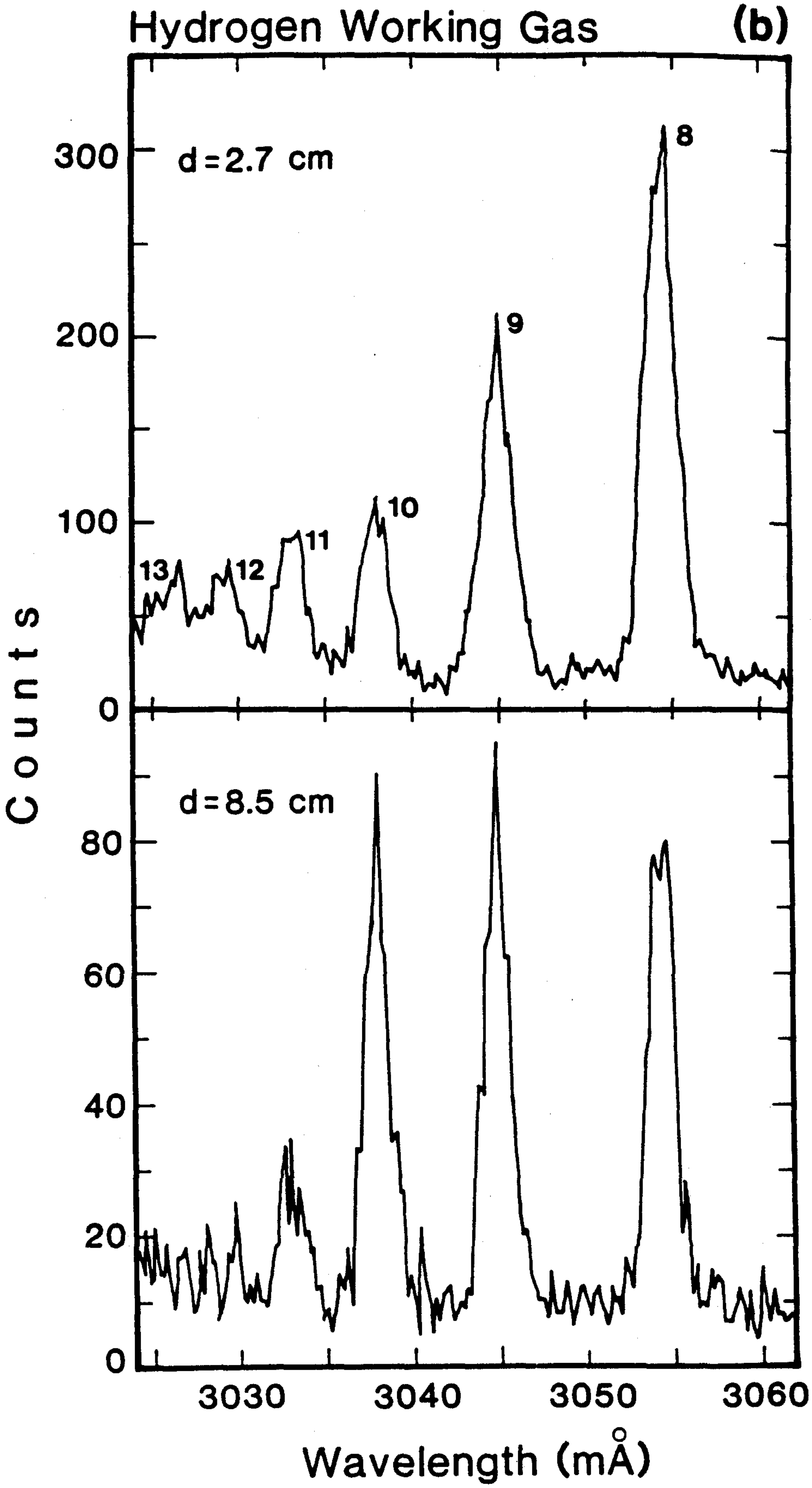
Hydrogen Working Gas
(b)
d=2.7 cm
d=8.5 cm
13
12
11
10
9
8
Counts
0
100
200
300
0
20
40
60
80
3030
3040
3050
3060
Wavelength (mÅ)

Figure 11(b)

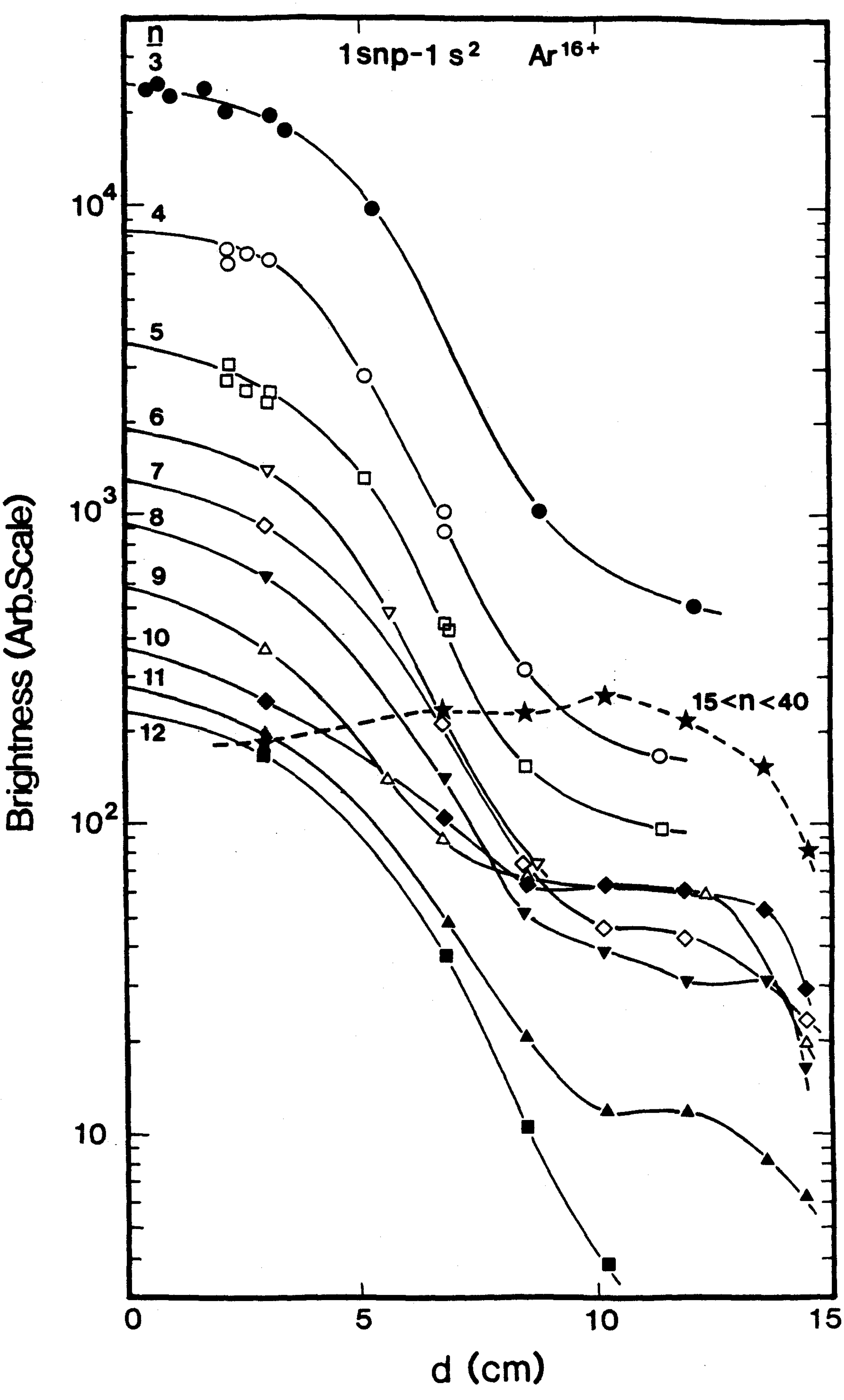

1snp-1s2 Ar16+
n
3
4
5
6
7
8
9
10
11
12
15<n<40
10^4
10^3
10^2
10
Brightness (Arb.Scale)
0
5
10
15
d (cm)

Figure 12

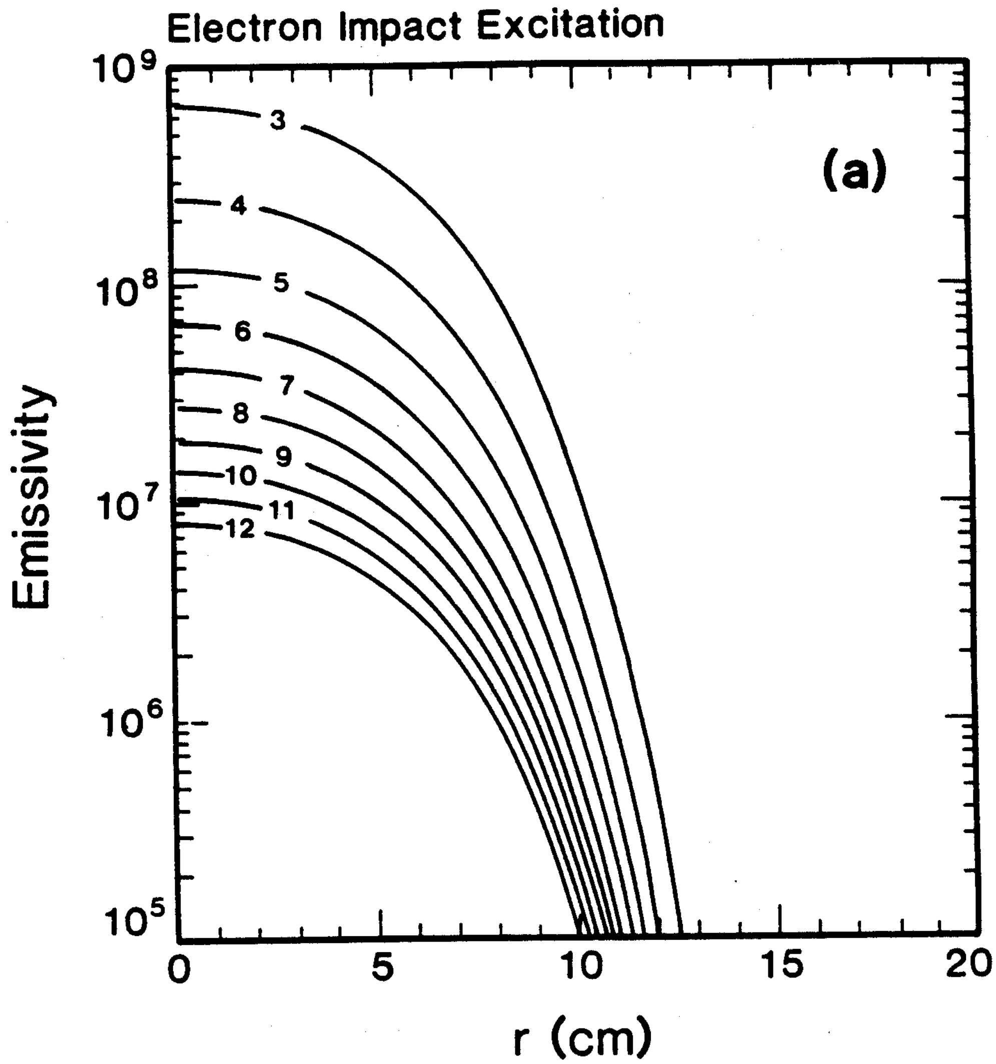
Electron Impact Excitation
(a)
Emissivity
r (cm)
3
4
5
6
7
8
9
10
11
12
10^9
10^8
10^7
10^6
10^5
0
5
10
15
20

Figure 13 (a)

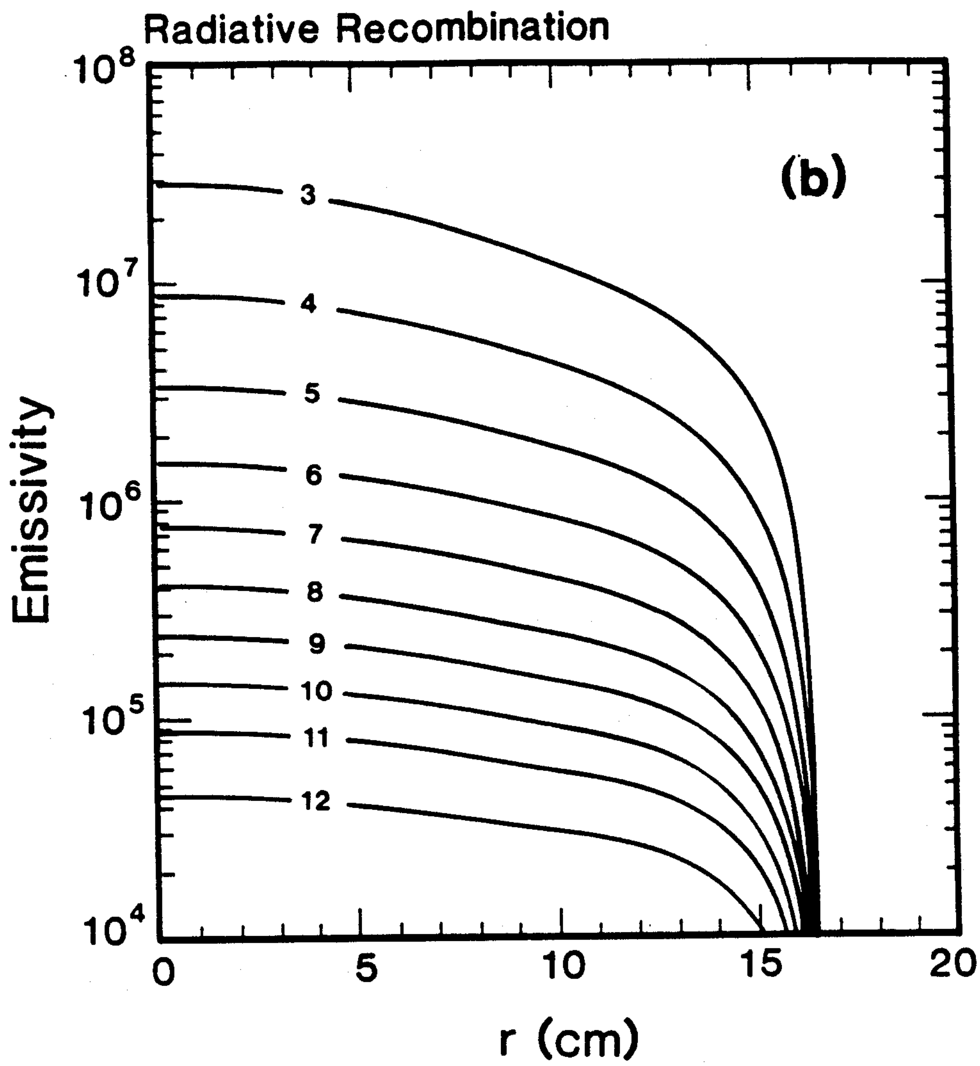
Radiative Recombination
(b)
Emissivity
r (cm)
10^8
10^7
10^6
10^5
10^4
0
5
10
15
20
3
4
5
6
7
8
9
10
11
12

Figure 13 (b)

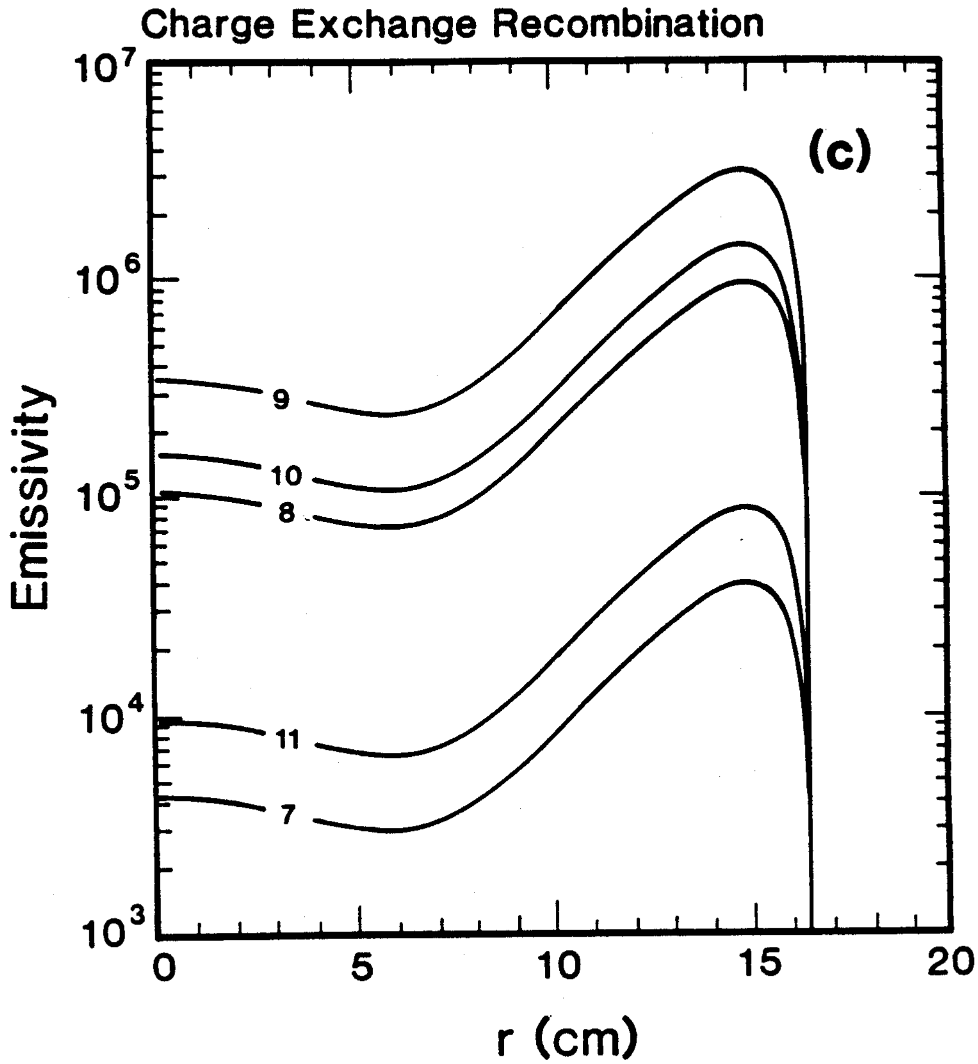

Charge Exchange Recombination
(c)
Emissivity
r (cm)
9
10
8
11
7
10^7
10^6
10^5
10^4
10^3
0
5
10
15
20

Figure 13 (c)

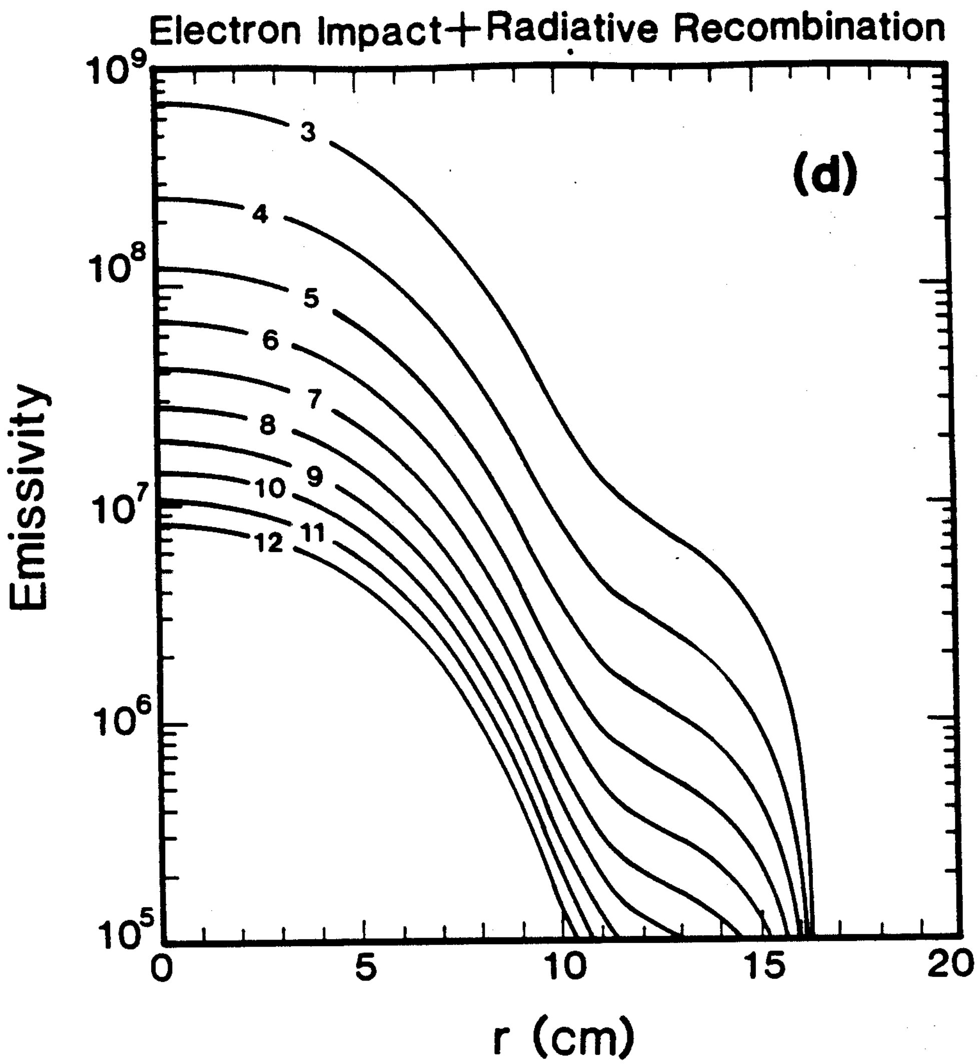
Electron Impact+Radiative Recombination
(d)
Emissivity
r (cm)
10^9
10^8
10^7
10^6
10^5
0
5
10
15
20
3
4
5
6
7
8
9
10
11
12

Figure 13 (d)

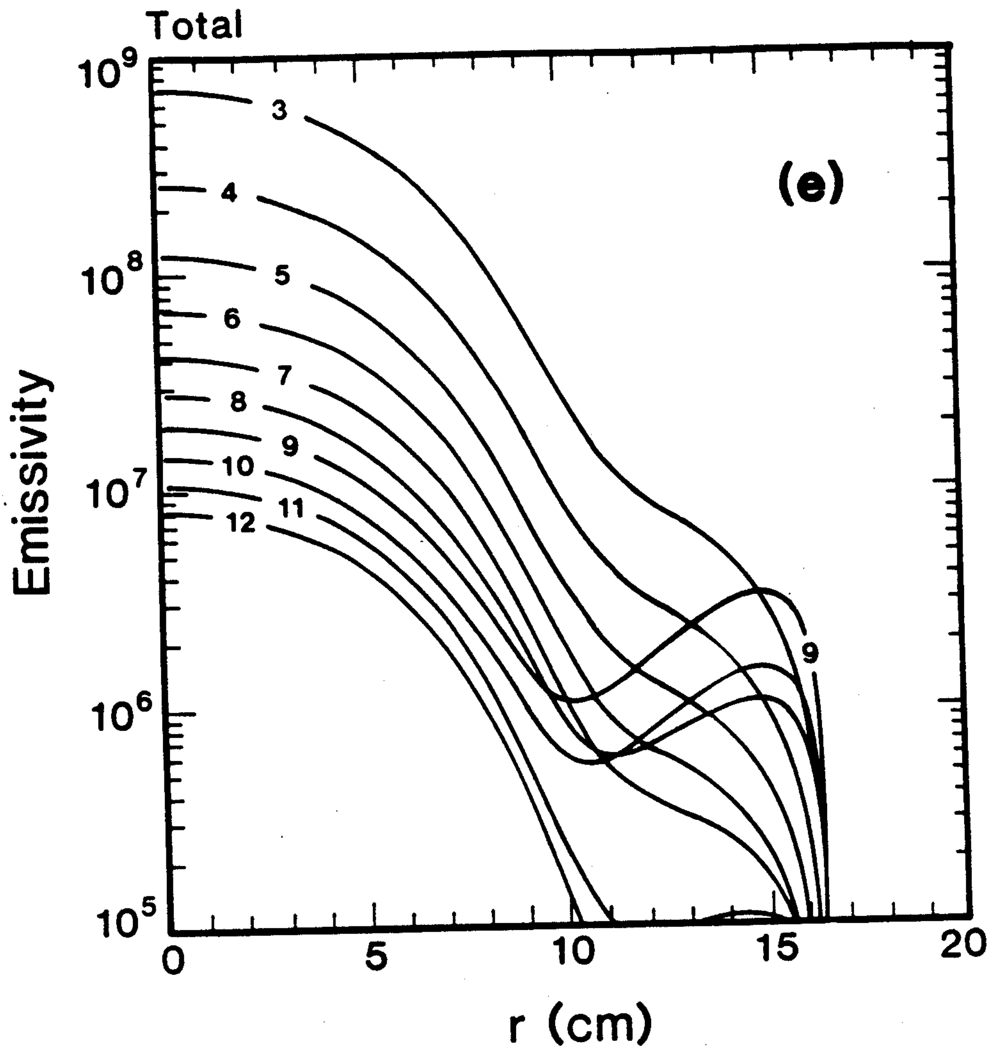
Total
10^9
10^8
10^7
10^6
10^5
(e)
3
4
5
6
7
8
9
10
11
12
9
Emissivity
0
5
10
15
20
r (cm)

Figure 13 (e)

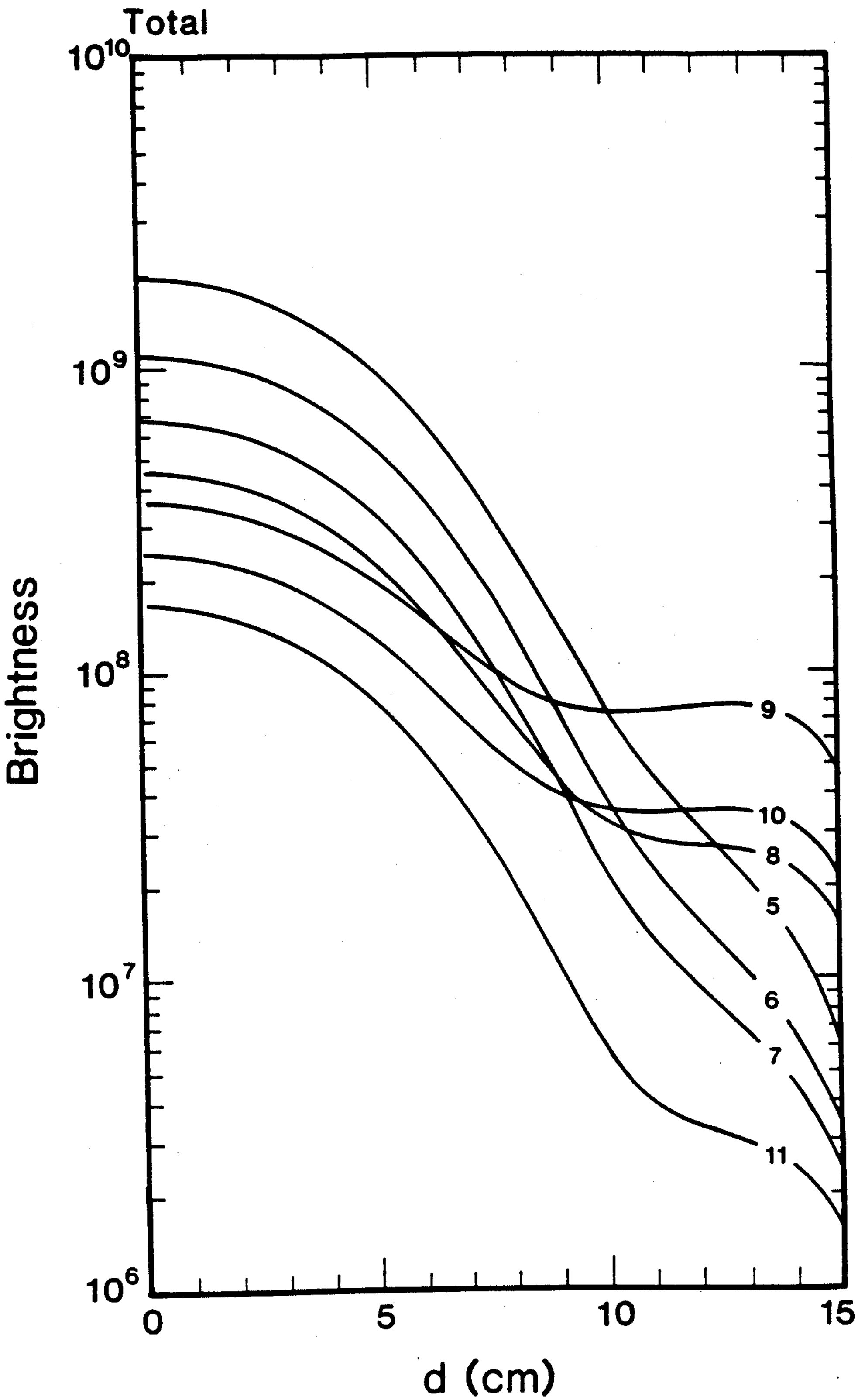

Figure 14

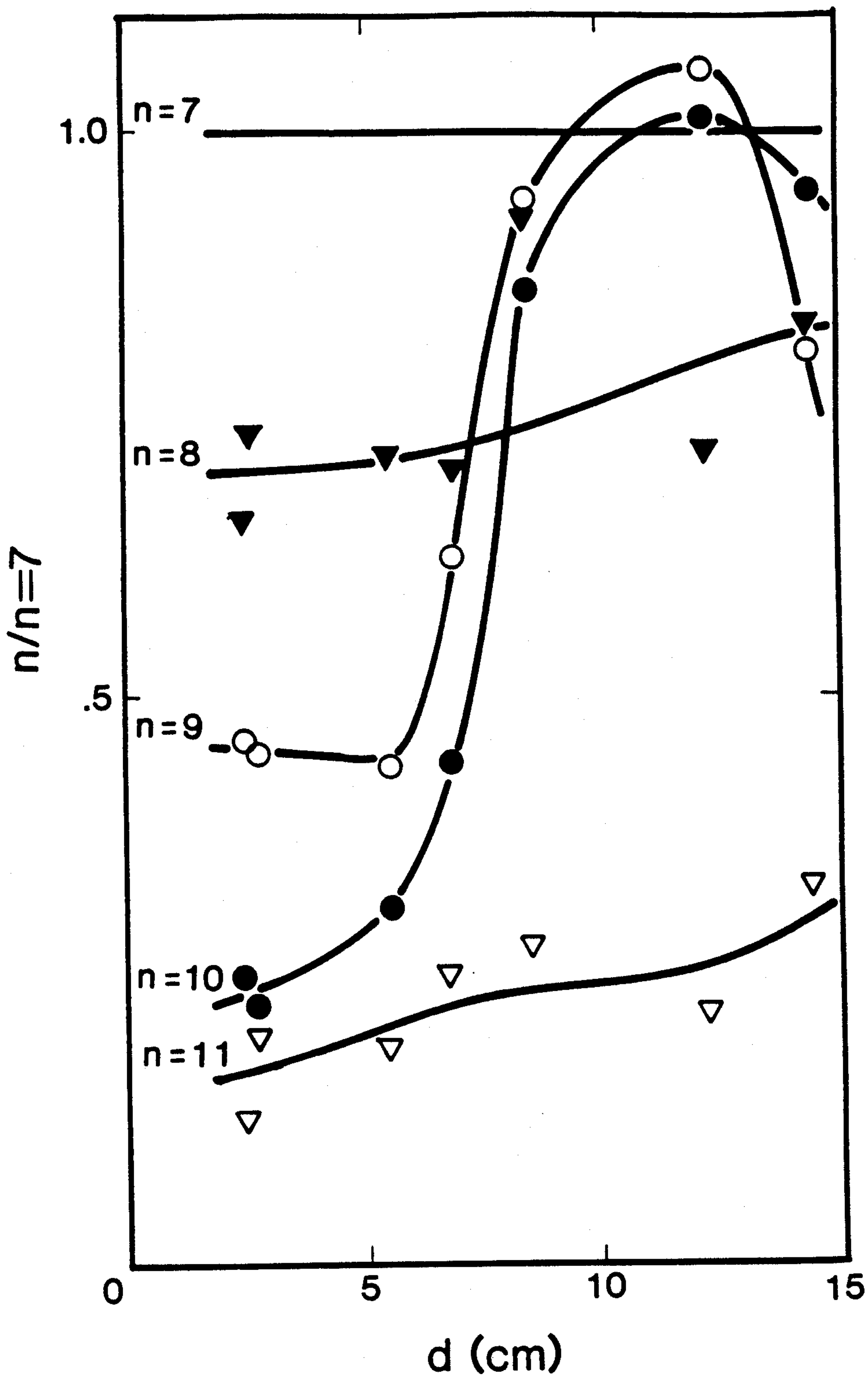

Figure 15

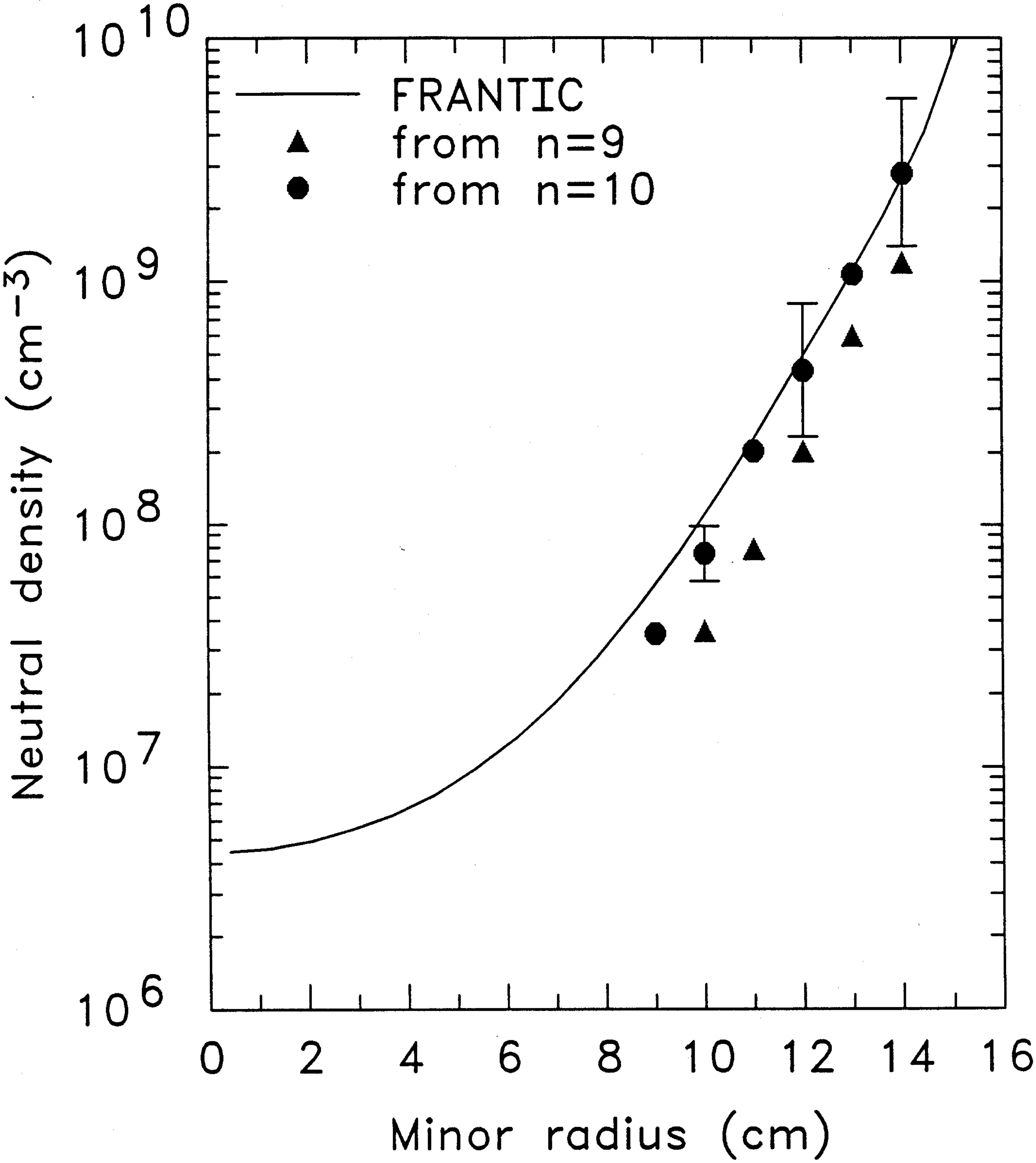

FRANTIC
from n=9
from n=10
Neutral density (cm^{-3})
10^{10}
10^{9}
10^{8}
10^{7}
10^{6}
0
2
4
6
8
10
12
14
16
Minor radius (cm)

Figure 16

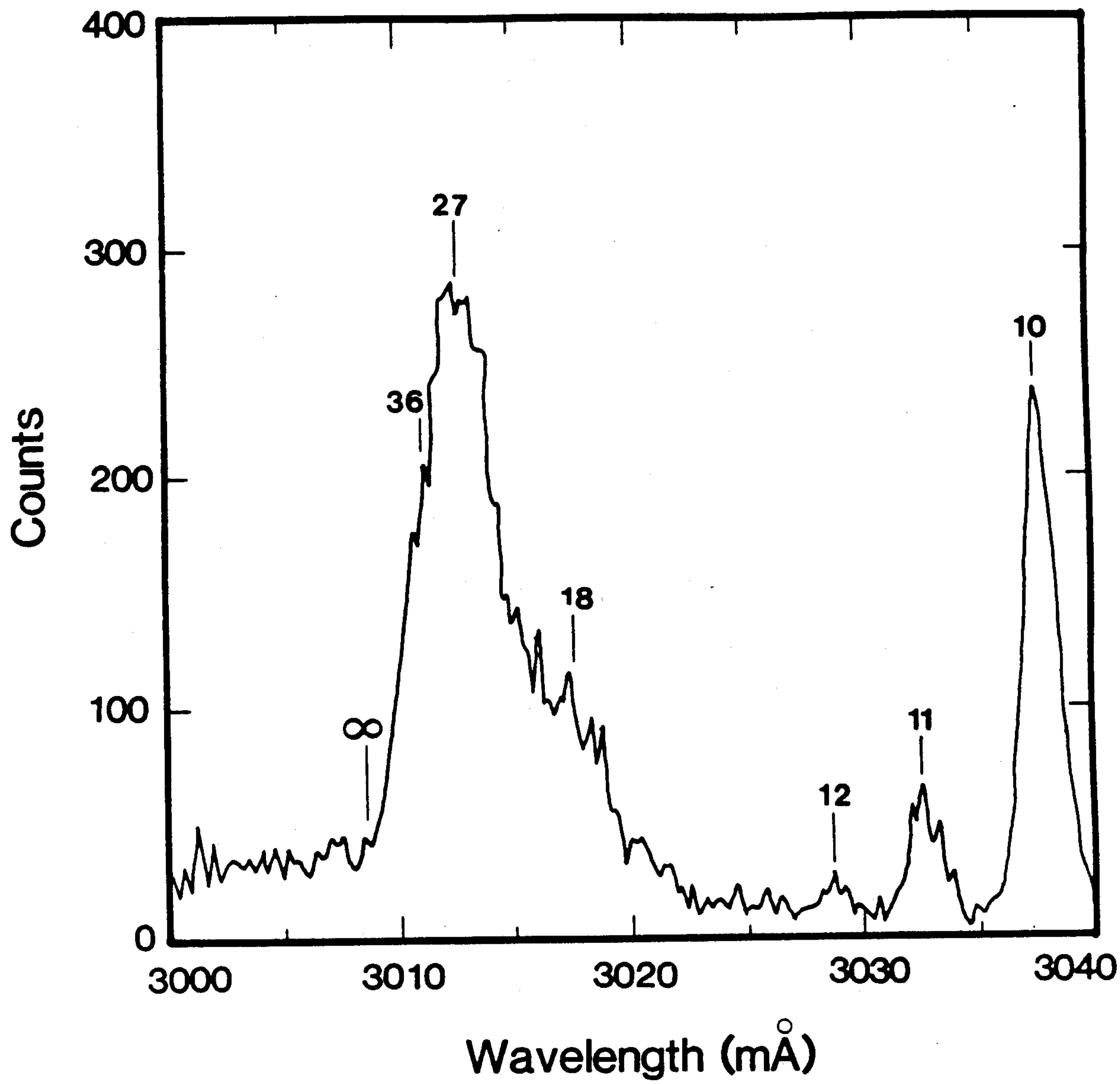

400
300
200
100
0
Counts
27
36
10
18
∞
11
12
3000
3010
3020
3030
3040
Wavelength (mÅ)

Figure 17

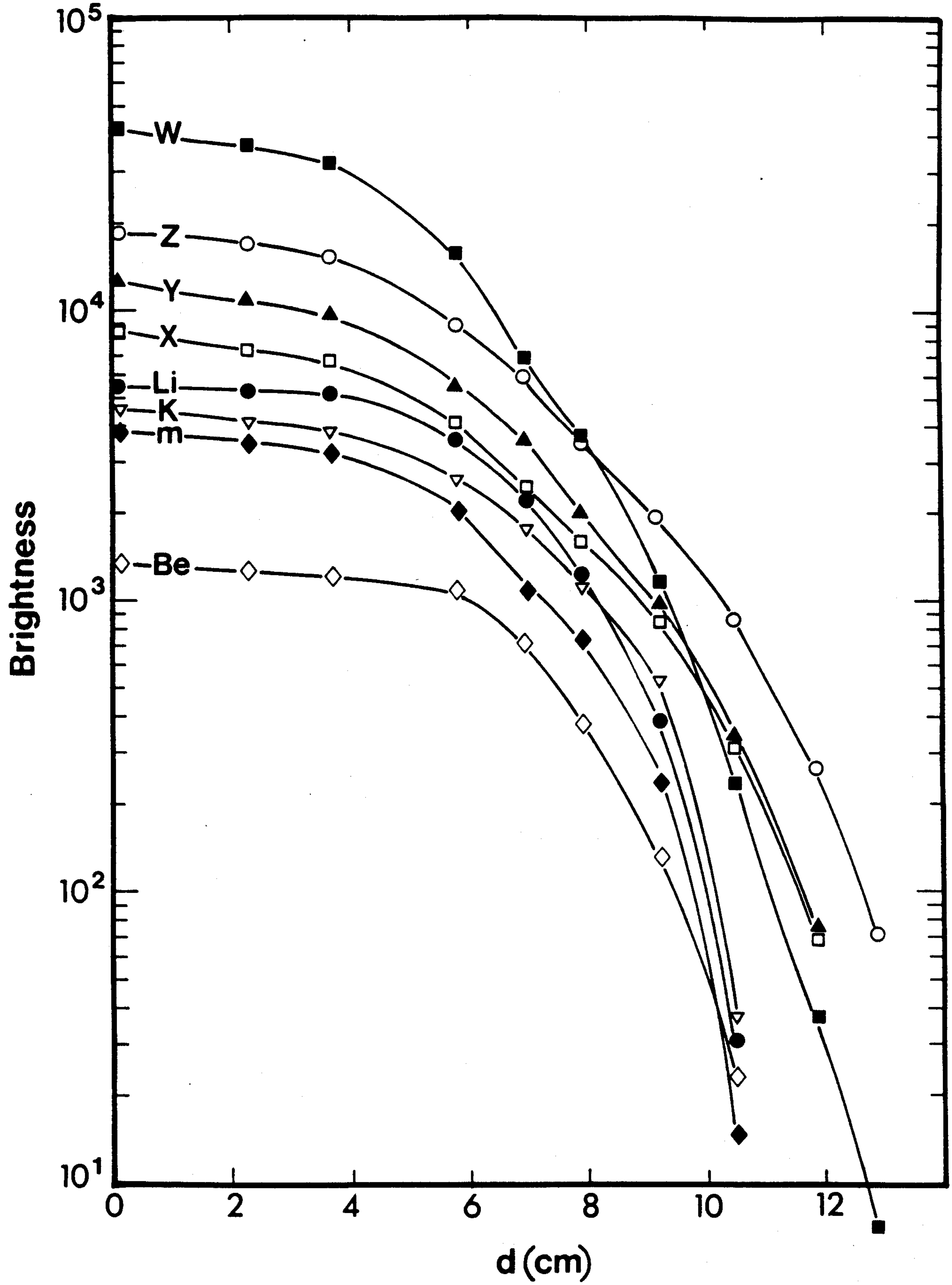

Figure 18

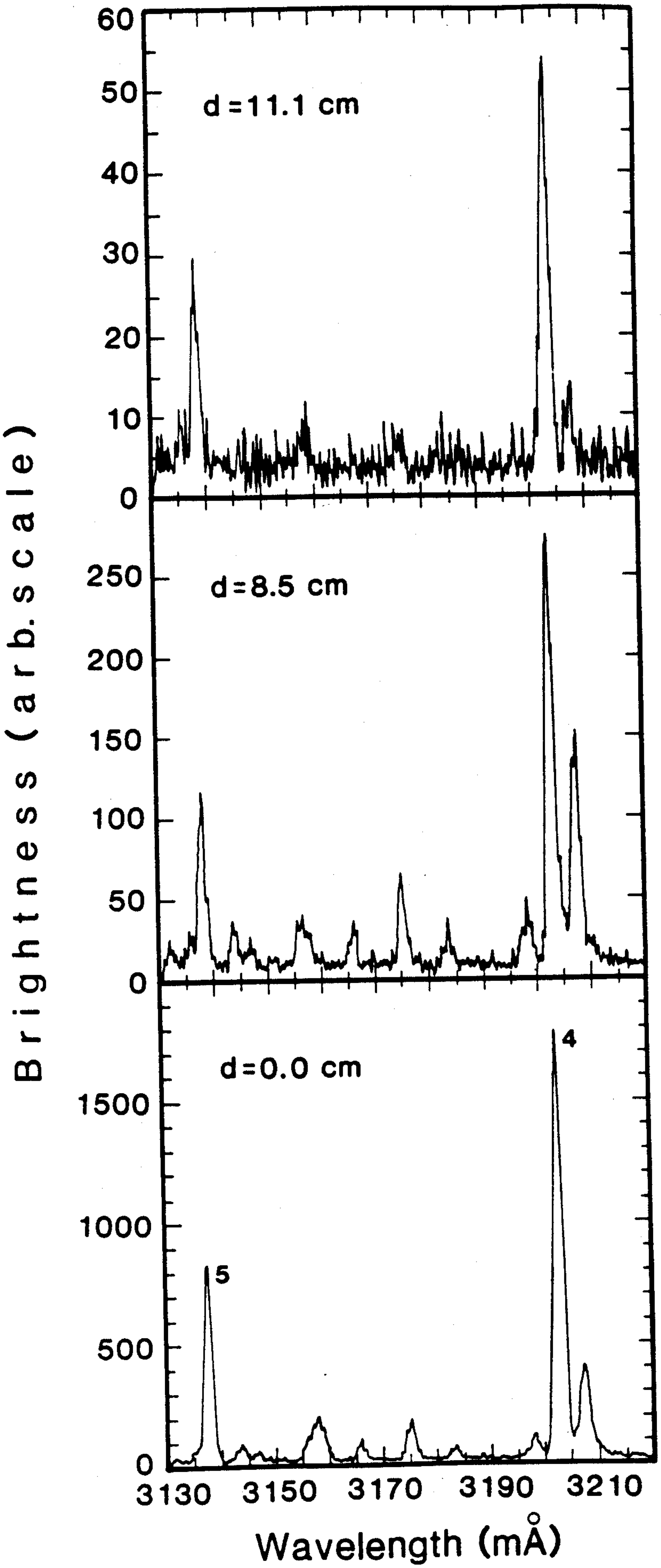
d=11.1 cm
d=8.5 cm
d=0.0 cm
5
4
60
50
40
30
20
10
0
250
200
150
100
50
0
1500
1000
500
0
3130
3150
3170
3190
3210
Brightness (arb. scale)
Wavelength (mÅ)

Figure 19

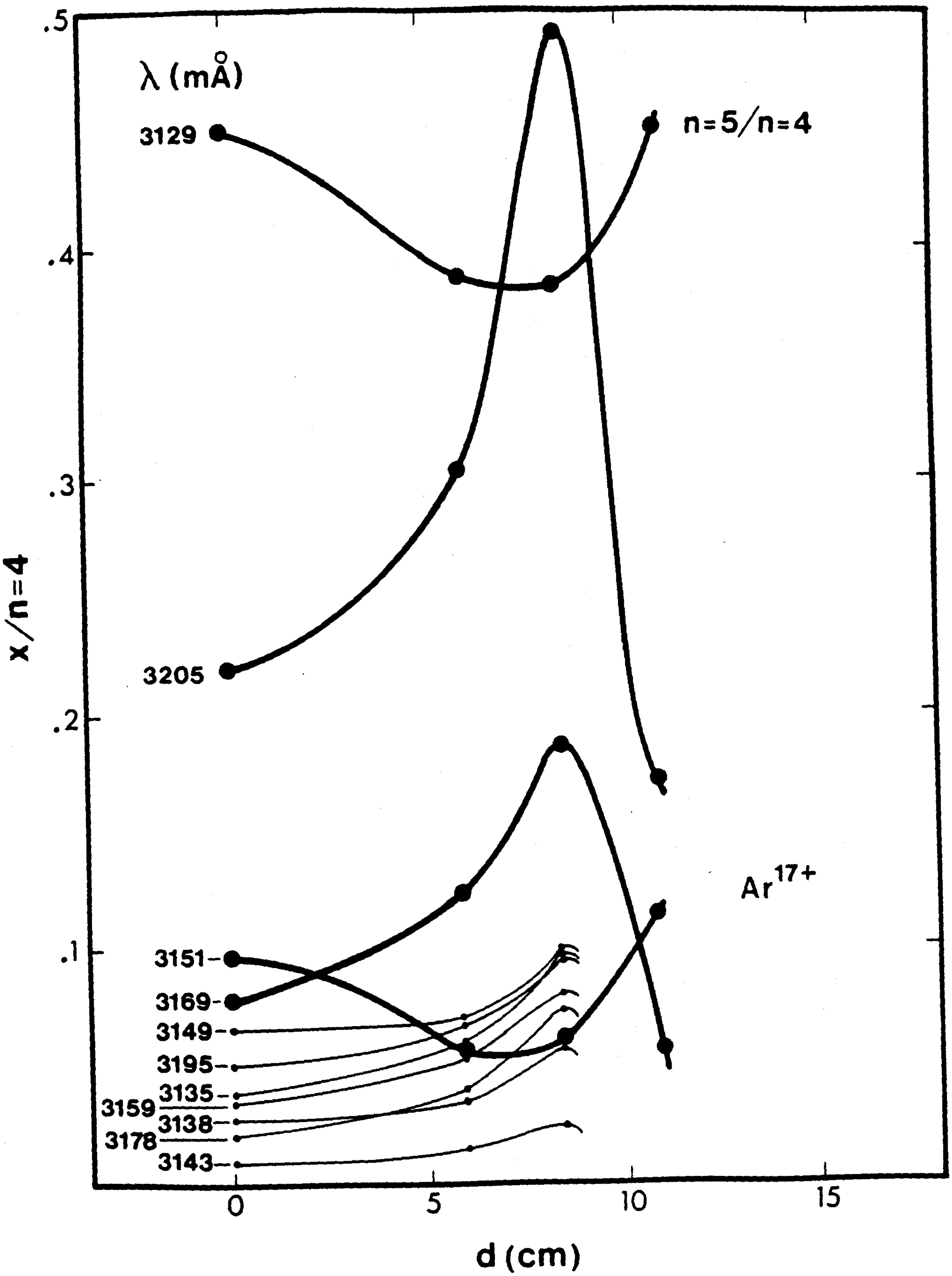
λ (mÅ)
n=5/n=4
3129
3205
Ar^{17+}
3151
3169
3149
3195
3135
3159
3138
3178
3143
.5
.4
.3
.2
.1
x/n=4
0
5
10
15
d (cm)

Figure 20